1977

The magnetic structure of metallic holmium as a function of temperature

Michael Joseph Pechan
Iowa State University

INFORMATION TO USERS

This material was produced from a microfilm copy of the original document. While the most advanced technological means to photograph and reproduce this document have been used, the quality is heavily dependent upon the quality of the original submitted.

The following explanation of techniques is provided to help you understand markings or patterns which may appear on this reproduction.

1. The sign or "target" for pages apparently lacking from the document photographed is "Missing Page(s)". If it was possible to obtain the missing page(s) or section, they are spliced into the film along with adjacent pages. This may have necessitated cutting thru an image and duplicating adjacent pages to insure you complete continuity.

2. When an image on the film is obliterated with a large round black mark, it is an indication that the photographer suspected that the copy may have moved during exposure and thus cause a blurred image. You will find a good image of the page in the adjacent frame.

3. When a map, drawing or chart, etc., was part of the material being photographed the photographer followed a definite method in "sectioning" the material. It is customary to begin photoing at the upper left hand corner of a large sheet and to continue photoing from left to right in equal sections with a small overlap. If necessary, sectioning is continued again — beginning below the first row and continuing on until complete.

4. The majority of users indicate that the textual content is of greatest value, however, a somewhat higher quality reproduction could be made from "photographs" if essential to the understanding of the dissertation. Silver prints of "photographs" may be ordered at additional charge by writing the Order Department, giving the catalog number, title, author and specific pages you wish reproduced.

5. PLEASE NOTE: Some pages may have indistinct print. Filmed as received.

University Microfilms International
300 North Zeeb Road
Ann Arbor, Michigan 48106 USA
St. John's Road, Tyler's Green
High Wycombe, Bucks, England HP10 8HR

The magnetic structure of metallic holmium as a function of temperature

by

Michael Joseph Pechan

A Dissertation Submitted to the
Graduate Faculty in Partial Fulfillment of
The Requirements for the Degree of
DOCTOR OF PHILOSOPHY

Department: Physics
Major: Solid State Physics

Approved:

Signature was redacted for privacy.

In Charge of Major Work

Signature was redacted for privacy.

For the Major Department

Signature was redacted for privacy.

For the Graduate College

Iowa State University
Ames, Iowa

1977

TABLE OF CONTENTS

LIST OF FIGURES

LIST OF TABLES

CHAPTER I. INTRODUCTION AND THEORY

The Neutron

The neutron is a nucleon and has a magnetic moment, and therefore interacts with matter via the nuclear and magnetic interactions. It suffices in thermal neutron scattering to view the neutron-nuclear interaction as a collision between solid spheres because the interaction is very short range ($\simeq 10^{-13}$ cm) and very strong. The nuclear property of the neutron is useful in neutron scattering to determine positions and motions of nuclei in a solid. The present work measures the nuclear interaction primarily for use as a reference for bringing the measured magnetic interaction to an absolute scale.

The focus here is upon the magnetic moment of the neutron and its interaction with a solid. The neutron has no measurable net charge but possesses a magnetic dipole moment of $-1.91\ \mu_N$ and a spin quantum number of $\frac{1}{2}$, where:

$$\mu_N = \text{nuclear magneton} = \frac{e\hbar}{2m_p c} \tag{1.1}$$

e = electronic charge

$\hbar = \dfrac{\text{Planck's constant}}{2\pi}$

m_p = proton rest mass

c = velocity of light in a vacuum.

Neutrons scattered elastically from a solid produce a diffraction pattern. This pattern reflects the symmetry of the solid and is directly related to the atomic and magnetic structure of the solid.

The Neutron Interaction with the Solid

The atoms in solid holmium form a hexagonal close packed (hcp) structure characterized by lattice parameters c and a (see Figure 1.1). Given the structure and these lattice parameters one can calculate the separation distances between parallel planes of atoms in the solid and also the angle between non-parallel planes of atoms. For example, for the hcp structure the distance between planes is given by

$$\frac{1}{d} = \left(\frac{4}{3} \frac{h^2+hk+k^2}{a^2} + \frac{\ell^2}{c^2} \right)^2 , \tag{1.2}$$

where h, k and ℓ are integers called Miller indices. Each plane of atoms in the lattice is identified by a set of these indices. See the Appendix for an explanation of reciprocal space. The angle between atomic planes (h_1, k_1, ℓ_1) and (h_2, k_2, ℓ_2) is given by

$$\cos\phi = \frac{h_1 h_2 + k_1 k_2 + \frac{1}{2}(h_1 k_2 + h_2 k_1) + \frac{3a^2}{4c^2}\ell_1 \ell_2}{\left[\left(h_1^2 + k_1^2 + h_1 k_1 + \frac{3a^2}{4c^2}\ell_1^2 \right) \left(h_2^2 + k_2^2 + h_2 k_2 + \frac{3a^2}{4c^2}\ell_2^2 \right) \right]^{\frac{1}{2}}} \tag{1.3}$$

Let us now examine coherent elastic scattering of a neutron beam from parallel planes in a solid (see Figure 1.2). Consider the neutron beam to be a plane wave with wavelength λ. The wave reflected from the upper plane interferes constructively with the wave reflected from the lower plane only if the following condition is satisfied

$$n\lambda = 2d\sin\theta \quad \text{(Bragg's law)}. \tag{1.4}$$

Bragg's law gives the positions of the diffraction peaks but does not give any information about the relative intensities of coherent reflections. These relative intensities will be given by adding the phases of

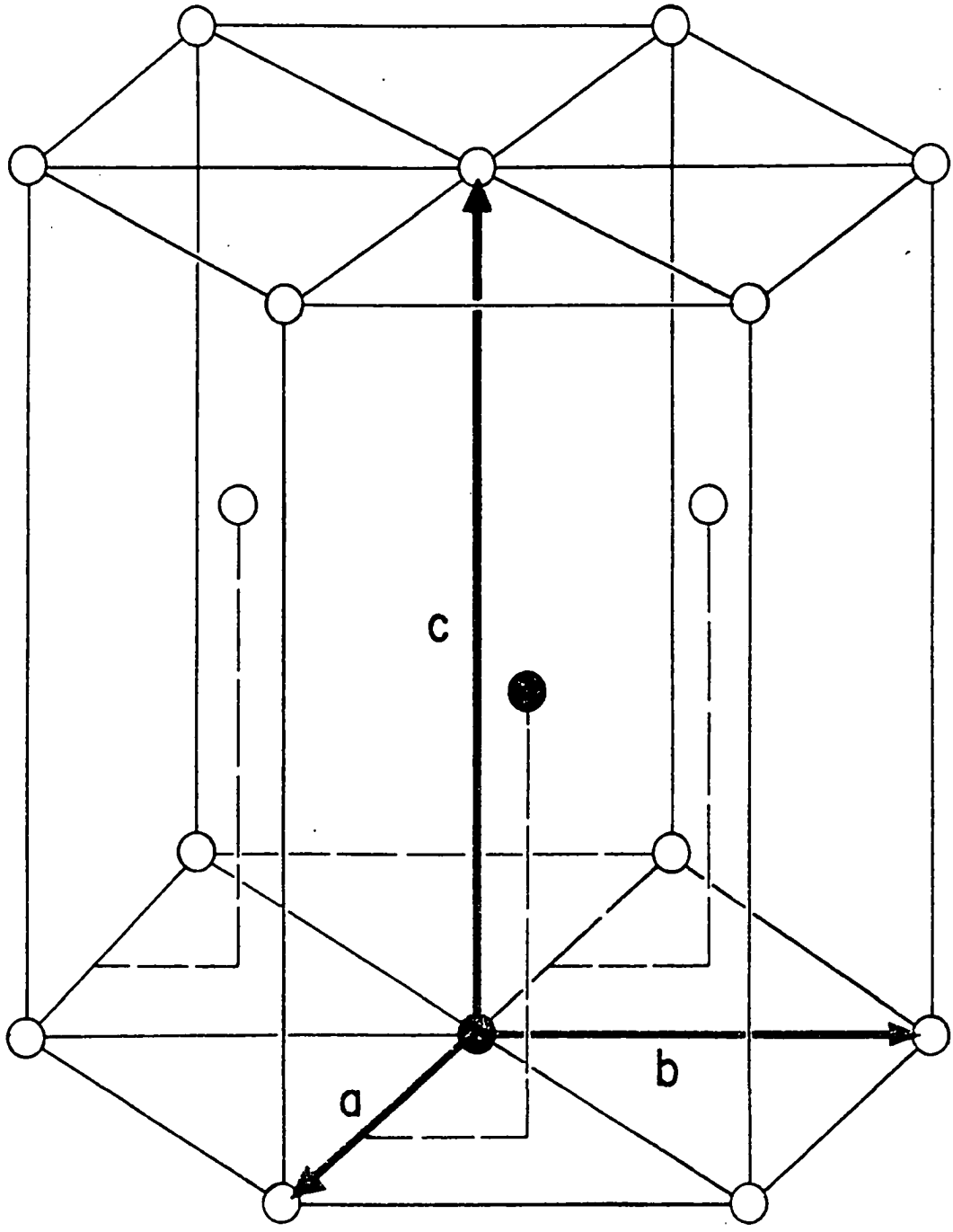

Figure 1.1. hcp Structure

the scattered radiation from each scattering center in the unit cell for a given plane of atoms. Consider only the nuclear contribution here and write the structure factor as

$$F_{nuclear} = -b_{coherent} \sum_n \exp\left[2\pi i\left(\frac{hx_n}{a}+\frac{ky_n}{b}+\frac{\ell z_n}{c}\right)\right] \qquad (1.5)$$

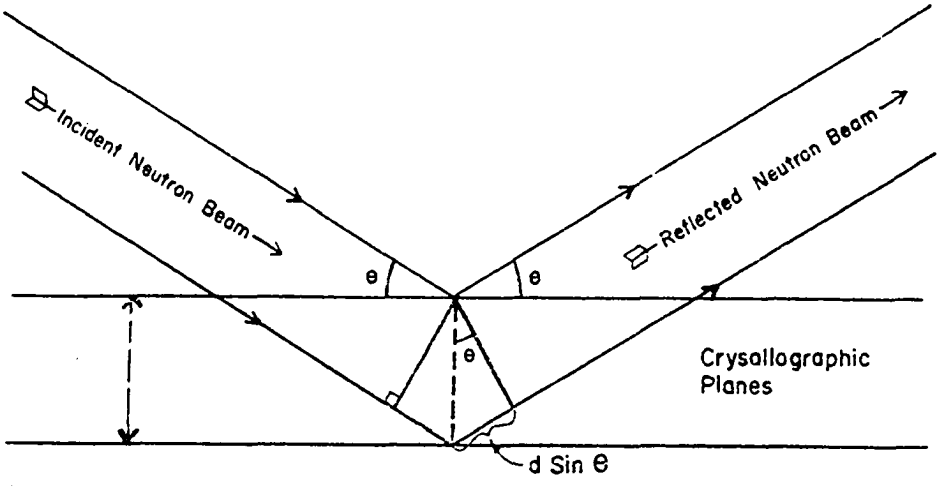

Bragg's Law → $n\lambda = 2d \sin\theta$

Figure 1.2. Coherent elastic scattering from a single crystal

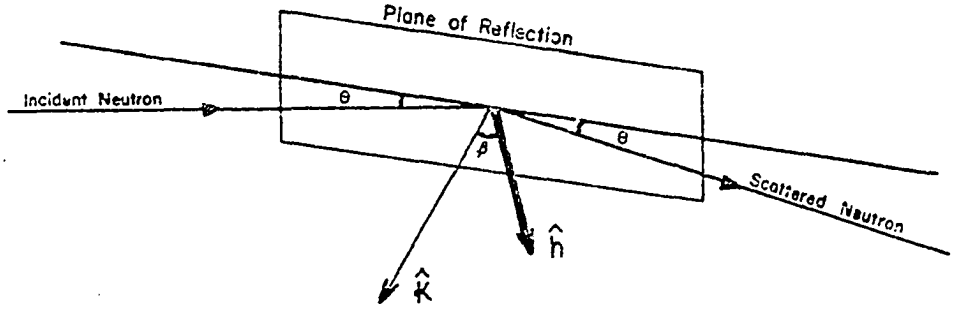

$$\vec{q} = \hat{K}\cdot(\hat{K}\cdot\hat{h}) - \hat{h}$$

Figure 1.3. Magnetic scattering of neutrons

where: (1) h,k,ℓ define the plane being considered (see Appendix A);

(2) x_n, y_n and z_n are the positions of the scattering centers in the unit cell (these are given in terms of $\vec{a}$, $\vec{b}$ and $\vec{c}$, the unit cell translation vectors);

(3) the sum is over the number of atoms in the unit cell;

(4) $b_{coherent}$ is the coherent nuclear scattering amplitude.

Upon multiplying the structure factor by its complex conjugate one obtains

$$F^2 = b^2_{coh.}\ G^2_{hk\ell} \tag{1.6}$$

where $G^2_{hk\ell}$ is the geometrical structure factor and is dependent upon the type of structure the atoms form in the solid. For example, for hcp the structure factor obeys the following selection rules:

	$G^2_{hk\ell}$
$h+2k = 3n$ and ℓ = even	4
$h+2k = 3n$ and ℓ = odd	0
$h+2k = 3n\pm1$ and ℓ = odd	3
$h+2k = 3n\pm1$ and ℓ = even	1

A magnetic structure in the solid can alter the nuclear diffraction pattern by introducing additional peaks in the pattern or by altering the intensities of existing nuclear peaks. Let's examine the case of a ferromagnet where each lattice site (atom) has the same magnetic moment and all moments are aligned (parallel). In this case the magnetic unit cell is the same as the chemical unit cell and the magnetic reflections will appear superimposed upon the nuclear reflections. Another classic structure to consider is the simple antiferromagnet, where the moments on each

atom are of the same magnitude but the moment direction is antiparallel from one layer to the next in a certain crystallographic direction. The magnetic unit cell is now twice as large as the chemical unit cell and "super lattice" magnetic reflections will appear. Also certain nuclear peaks will have magnetic reflections superimposed upon them.

One structure which is very important for the interpretation of our measurements is the spiral spin structure. In this structure the moments form ferromagnetic sheets in the basal plane, with the moments in a given layer rotated by an angle, ϕ_L, with respect to the moments in the layer below it (see Figure 1.4). In this helical antiferromagnetic structure the magnetic unit cell is several times larger than the chemical unit cell and magnetic reflections appear as satellites about each nuclear reflection. Because the moments lie in the basal plane and the modulation is along the c axis of the spiral, the magnetic satellites appear, on either side of all nuclear peaks, in the $[00\ell]$ direction (see Figure 2.6). Since the modulation is purely sinusoidal there is only one term in the Fourier transform from real space to reciprocal space and therefore only the first order magnetic satellites are present. As the basal plane moment increases, the periodicity of the spiral deviates from purely sinusoidal and higher order terms are present in the Fourier transform. These higher order terms appear as fifth and seventh order satellites in the diffraction pattern.

Higher order multipoles in the atomic form factor modulate the magnetic structure in such a way as to produce very weak third order satellites in the neutron diffraction pattern.

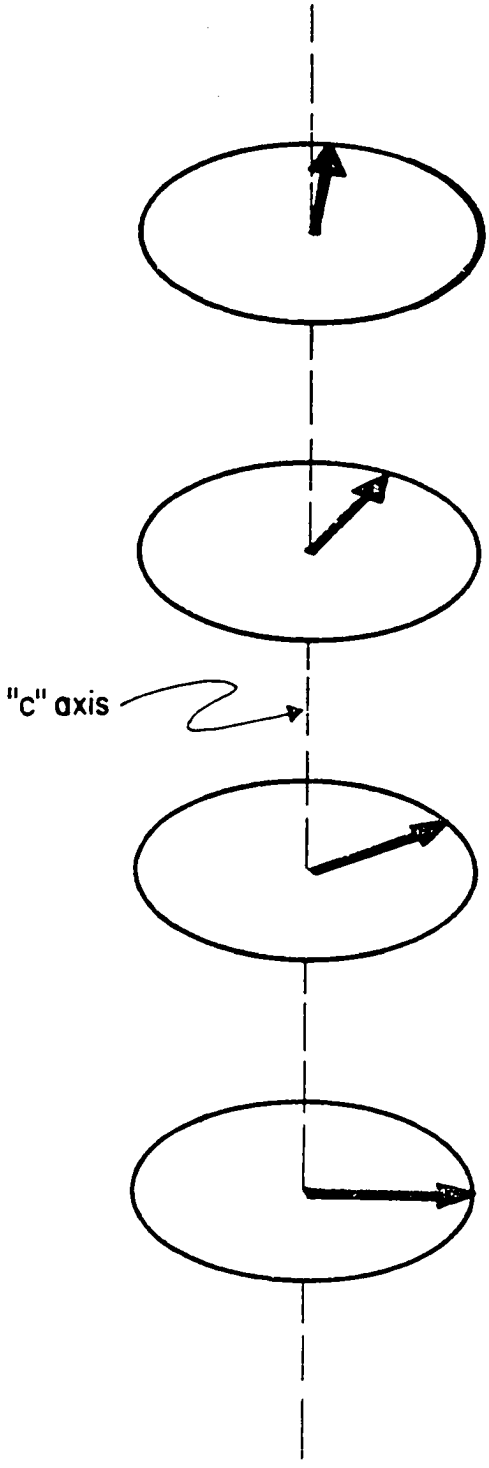

Figure 1.4. Simple helical structure

The Neutron Interaction with the Magnetic Structure

The formulation of the magnetic scattering amplitude of the tri-positive holmium ion will be presented first. Then this holmium ion will be placed in a simple, magnetic spiral structure and the resulting structure factor will be calculated. Finally the magnetic structure factor will be calculated for the "bunched" spiral structure.

Let us now formulate the neutron interaction with one ion. The cross section for elastic coherent scattering is given by:

$$\frac{d\sigma}{d\Omega} = |f(\theta)|^2 \tag{1.7}$$

where:

$$f(\theta) = f_{nuclear} + f_{magnetic} = \text{scattering amplitude.} \tag{1.8}$$

$f(\theta)$ is, in general, a function of θ, the scattering angle. Now

$$f_{nuclear} = -b, \tag{1.9}$$

where $\underline{b}$ is an experimentally determined quantity and the minus sign is chosen to make an attractive potential have a positive scattering amplitude. Note that the nuclear scattering amplitude is independent of scattering angle (isotropic).

The magnetic scattering amplitude is given by

$$f_{magnetic} = P(\theta)\ \vec{q}\cdot\vec{\sigma}, \tag{1.10}$$

where:

$$P(\theta) = \gamma\ r_o\, Sf, \tag{1.11}$$

$\gamma = -1.91\ \mu_N$ for neutrons,

r_o = classical electron radius,

S = angular momentum number of the atom,

f = atomic magnetic form factor (Fourier transform of the magnetization density);

$$\vec{q} = \hat{\kappa}(\hat{\kappa}\cdot\hat{h})-\hat{h} \quad \text{magnetic interaction vector (see Figure 1.3),} \tag{1.12}$$

$\hat{\kappa}$ = unit vector along the scattering vector (see Appendix A),

$\hat{h}$ = unit vector in the direction of the ionic moment,

$\vec{\sigma} = 2\vec{s}$ neutron Pauli spin matrix, $\vec{s} = \frac{1}{2}$ (for neutrons).

For unpolarized neutrons scattered coherently take the average of the following two processes: neutron spin parallel to $\vec{q}$ and neutron spin antiparallel to $\vec{q}$. Write the scattering amplitude as

$$f = -b+P(\theta)\ q\ \sigma_q \qquad \sigma_q = \pm 1. \tag{1.13}$$

The scattering cross section becomes

$$\frac{d\sigma}{d\Omega}_+ = (-b+Pq)^2, \tag{1.14}$$

$$\frac{d\sigma}{d\Omega}_- = (-b-Pq)^2, \tag{1.15}$$

and taking the average

$$\frac{1}{2}\frac{d\sigma}{d\Omega}_+ + \frac{1}{2}\frac{d\sigma}{d\Omega}_- = b^2+P^2q^2. \tag{1.16}$$

Therefore for unpolarized neutrons we can write the magnetic scattering length as a vector quantity

$$\vec{f}_{mag} = P(\theta)\ \vec{q} \tag{1.17}$$

The magnetic scattering amplitude will be calculated here using the fully relativistic magnetic multipoles calculated by Stassis, Deckman and Harmon[1]. The scattering amplitude is given by

$$P(\theta) = \gamma r_o \sum_k \left[\frac{2}{k(k+1)}\right]^{\frac{1}{2}} P_k'(\cos\beta)\ \langle \alpha J M | T_{k0}^{m} | \alpha J M \rangle \tag{1.18}$$

where: $k = 1,3, \ldots, 2\ell+1$ ($\ell = 3$ for holmium's 4f shell)

$P_k'(\cos\beta)$ = derivative of a Legendre Polynomial,

β is the angle between the moment direction and the scattering vector,

T_{k0}^{m} is the m=o component of the magnetic multipole of order k

k = 1 is a magnetic dipole,

k = 3 is a magnetic octupole, etc.

In this study the magnetic moment of the holmium ion is of interest Therefore I will write the spin explicitly in the expression for $P(\theta)$,

$$P(\theta) = \gamma r_o S \left[\sum_k \frac{1}{S}\left(\frac{2}{k(k+1)}\right)^{\frac{1}{2}} P_k'(\cos\beta) \langle \alpha J M | T_{k0}^{m} | \alpha J M \rangle\right] \tag{1.19}$$

The quantity in the square brackets is now the magnetic form factor, $f(\theta)$, which is normalized to 1 in the forward scattering direction. It is this term upon which we will now focus our attention.

The general matrix element above can be related to tabulated reduced matrix elements by a 3-j symbol[2] as

$$\langle \alpha J M | T_{k0}^{m} | \alpha J M \rangle = (-)^{J-M} \begin{pmatrix} J & K & J \\ -M & 0 & M \end{pmatrix} (\alpha J || T_{k0}^{m} || \alpha J) \qquad (1.20)$$

where $\begin{pmatrix} J & K & J \\ -M & 0 & M \end{pmatrix}$ is a 3-j symbol, and $(\alpha J || T_{k0}^{m} || \alpha J)$ is tabulated[1]. The 3-j symbol is merely a symmetric representation of Clebsch-Gordan coefficients. Because of the strong spin-orbit interaction in rare earth metals one would expect that M=J (for holmium J=8). The 3-j symbols become[3]

$$\begin{pmatrix} 8 & 1 & 8 \\ -8 & 0 & 8 \end{pmatrix} = \left[\frac{8}{153}\right]^{\frac{1}{2}}, \qquad (1.21a)$$

$$\begin{pmatrix} 8 & 3 & 8 \\ -8 & 0 & 8 \end{pmatrix} = \left[\frac{28}{969}\right]^{\frac{1}{2}}, \qquad (1.21b)$$

$$\begin{pmatrix} 8 & 5 & 8 \\ -8 & 0 & 8 \end{pmatrix} = \left[\frac{104}{10,659}\right]^{\frac{1}{2}}, \qquad (1.21c)$$

$$\begin{pmatrix} 8 & 7 & 8 \\ -8 & 0 & 8 \end{pmatrix} = \left[\frac{130}{66,861}\right]^{\frac{1}{2}}, \qquad (1.21d)$$

The derivatives of the Legendre Polynomials are

$$P_1'(\cos\beta) = 1, \qquad (1.22a)$$

$$P_3'(\cos\beta) = \frac{3}{2}(5\cos^2\beta - 1), \qquad (1.22b)$$

$$P_5'(\cos\beta) = \frac{15}{8}(21\cos^4\beta - 14\cos^2\beta + 1), \qquad (1.22c)$$

$$P_7'(\cos\beta) = \frac{7}{16}(429\cos^6\beta + 495\cos^4\beta + 135\cos^2\beta - 5). \qquad (1.22d)$$

The form factor now can be expressed as

$$f(\theta) = aT_1^m + b(5\cos^2\beta - 1)T_3^m + c(21\cos^4\beta - 14\cos^2\beta + 1)T_5^m + d(429\cos^6\beta - 495\cos^4\beta + 135\cos^2\beta - 5)T_7^m \quad (1.23)$$

where,

$$a = \left[\frac{8}{153}\right]^{\frac{1}{2}}, \quad (1.24a)$$

$$b = \frac{3}{2}\left[\frac{1}{6}\right]^{\frac{1}{2}}\left[\frac{28}{969}\right]^{\frac{1}{2}}, \quad (1.24b)$$

$$c = \frac{15}{8}\left[\frac{1}{15}\right]^{\frac{1}{2}}\left[\frac{104}{10,659}\right]^{\frac{1}{2}}, \quad (1.24c)$$

$$d = \frac{7}{16}\left[\frac{1}{28}\right]^{\frac{1}{2}}\left[\frac{130}{66,861}\right]^{\frac{1}{2}}, \quad (1.24d)$$

and T_k^m are short for $(\alpha J||T_{k0}^m||\alpha J)$. So one can write

$$f(\theta) = A + B\cos^2\beta + C\cos^4\beta + D\cos^6\beta \quad (1.25)$$

where,

$$A = aT_1^m - bT_3^m + cT_5^m - 5dT_7^m, \quad (1.26a)$$

$$B = 5bT_3^m - 14cT_5^m + 135dT_7^m, \quad (1.26b)$$

$$C = 21cT_5^m - 495dT_7^m, \quad (1.26c)$$

$$D = 429dT_7^m. \quad (1.26d)$$

In the above treatment the neutron beam is interacting with a single magnetic ion. Consider now an ion in a magnetic spiral structure

and make a transformation from β, the angle between the moment and scattering vector, to ϕ, the angle between the c axis and the scattering vector and ϕ_L, the turn angle between moments of successive layers (see Figure 1.5)

$$\cos\beta = \sin\phi \cos\phi_L . \tag{1.27}$$

The form factor becomes

$$f(\theta) = A + B\sin^2\phi \cos^2\phi_L + C\sin^4\phi \cos^4\phi_L + D\sin^6\phi \cos^6\phi_L . \tag{1.28}$$

Write

$$\cos^2\phi_L = \frac{\cos(2\phi_L) + 1}{2} , \tag{1.29a}$$

$$\cos^4\phi_L = \frac{1}{4}\left[\frac{\cos(4\phi_L)}{2} + 2\cos(2\phi_L) + \frac{3}{2}\right] , \tag{1.29b}$$

$$\cos^6\phi_L = \frac{1}{32}\left[\cos(6\phi_L) + 6\cos(4\phi_L) + 15\cos(2\phi_L) + 10\right] \tag{1.29c}$$

and the form factor becomes,

$$f(\theta) = \sum_{n=0}^{3} B_{2n} \cos(2n\phi_L) , \tag{1.30}$$

where

$$B_0 = aT_1^m + b\left(\frac{5}{2}\sin^2\phi - 1\right)T_3^m + c\left(\frac{63}{8}\sin^4\phi - 7\sin^2\phi + 1\right)T_5^m + \frac{d}{2}\left(\frac{5(429)}{8}\sin^6\phi - \frac{3(495)}{4}\sin^4\phi + 135\sin^2\phi - 10\right)T_7^m \tag{1.31a}$$

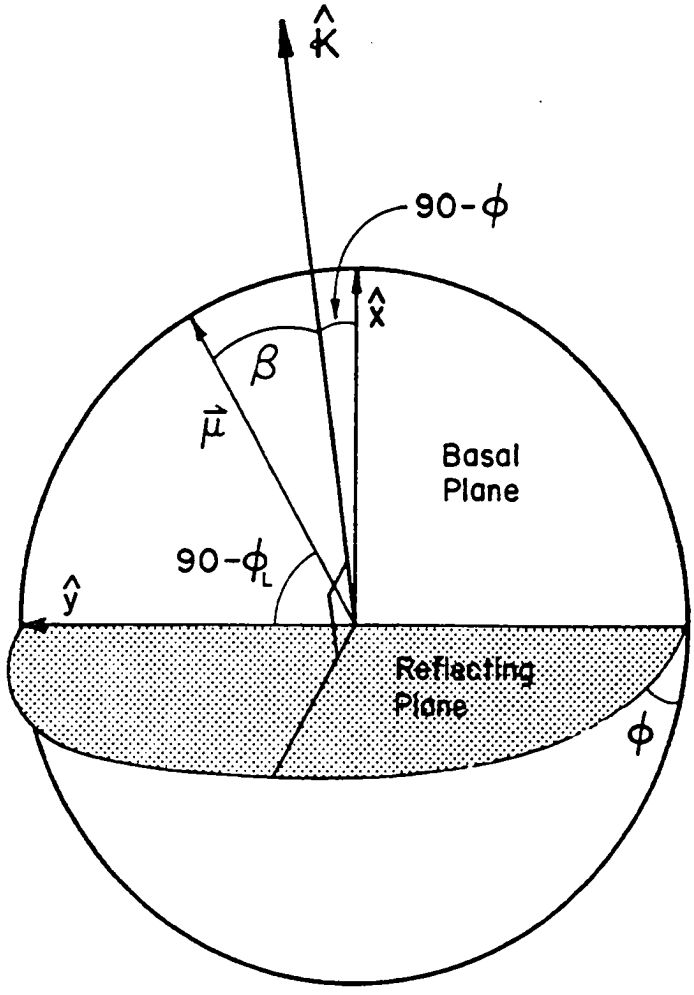

Figure 1.5. Transformation from β to ϕ and ϕ_L

$$B_2 = \frac{1}{2}\sin^2\phi\left[5bT_3^m + 7c(3\sin^2\phi - 2)T_5^m + d\left[\frac{5}{16}(429)\sin^4\phi - 495\sin^2\phi + 135\right]T_7^m\right] \quad (1.31b)$$

$$B_4 = \frac{1}{8}\sin^4\phi\left[21cT_5^m + d\left[\frac{3}{2}(429)\sin^2\phi - 495\right]T_7^m\right] \quad (1.31c)$$

$$B_6 = \frac{429}{32}d\sin^6\phi\, T_7^m. \quad (1.31d)$$

Let us now consider the total scattering cross section[4]

$$\frac{d\sigma}{d\Omega} = (\gamma r_o)^2 \sum_{jj'}\left[f_j(\theta)\, f_{j'}(\theta)\, e^{-i\vec{\kappa}\cdot(\vec{R}_j - \vec{R}_{j'})} \sum_{\alpha,\beta}(\delta_{\alpha\beta} - \hat{\kappa}_\alpha\hat{\kappa}_\beta)\langle S_j^\alpha S_{j'}^\beta\rangle\right], \quad (1.32)$$

where

the sum is over all atoms in the solid,

$f_j(\theta)$ is the atomic form factor of the j^{th} atom,

$\vec{\kappa}$ is the scattering vector,

$\vec{R}_j$ is the position of the j^{th} atom in the solid,

$\hat{\kappa}$ is the unit vector along the scattering vector,

$$\vec{S}_j = \frac{S}{2}(e^{-i\phi_L}\hat{m}^+ + e^{i\phi_L}\hat{m}^-), \quad (1.33)$$

$\hat{m}^\pm = \hat{m}_x \pm i\,\hat{m}_y$, $\hat{m}_{x,y}$ = unit vectors along $\hat{x}$ and $\hat{y}$ in the basal plane

S = magnitude of the spin in the basal plane.

Re-express the turn angle as

$$\phi_L = \vec{k}_o\vec{R}_j \quad (1.34)$$

where k_o is the wave vector of the magnetic spiral. With $\vec{S}_j$ written as it is in equation (1.33) the sum over α and β may be expressed as

$$\sum_{\alpha,\beta} (\delta_{\alpha,\beta} - \kappa_\alpha \kappa_\beta) \langle S_j^\alpha S_{j'}^\beta \rangle =$$

$$\frac{1}{4} S^2 (1 + \cos^2\phi) \left[e^{-i\vec{k}_o \cdot (\vec{R}_j + \vec{R}_{j'})} + e^{i\vec{k}_o \cdot (\vec{R}_j - \vec{R}_{j'})} \right.$$

$$\left. + e^{i\vec{k}_o \cdot (\vec{R}_j + \vec{R}_{j'})} + e^{-i\vec{k}_o \cdot (\vec{R}_j + \vec{R}_{j'})} \right] . \qquad (1.35)$$

The $(1 + \cos^2\phi)$ term provides for the projection of the basal plane moment onto the reflecting plane. The form factor can be rewritten

$$f_j(\theta) = \sum_{n=0}^{3} B_{2n} \cos(2n\, \vec{k}_o \cdot \vec{R}_j) =$$

$$\sum_{n=0}^{3} \frac{B_{2n}}{2} \left(e^{i2n\vec{k}_o \cdot \vec{R}_j} + e^{-i2n\vec{k}_o \cdot \vec{R}_{j'}} \right) \qquad (1.36)$$

and the total scattering cross section becomes

$$\frac{d\sigma}{d\Omega} = (\gamma r_o)^2 S^2 \; \frac{1 + \cos^2\phi}{4} \sum_{jj'} \left[\sum_n B_{2n} \frac{\left(e^{i2n\vec{k}_o \cdot \vec{R}_j} + e^{-i2n\vec{k}_o \cdot \vec{R}_{j'}} \right)}{2} \right]$$

$$X \left[\sum_n B_{2n} \frac{\left(e^{i2n\vec{k}_o \cdot \vec{R}_{j'}} + e^{-i2n\vec{k}_o \cdot \vec{R}_{j'}} \right)}{2} \right] \left[e^{-i\vec{\kappa} \cdot (\vec{R}_j - \vec{R}_{j'})} \right] \left[e^{i\vec{k}_o \cdot (\vec{R}_j - \vec{R}_{j'})} \right.$$

$$\left. + e^{-i\vec{k}_o \cdot (\vec{R}_j - \vec{R}_{j'})} + e^{i\vec{k}_o \cdot (\vec{R}_j + \vec{R}_{j'})} + e^{-i\vec{k}_o \cdot (\vec{R}_j + \vec{R}_{j'})} \right] . \qquad (1.37)$$

Performing the multiplication and the sum over all atoms in the volume yields

$$\frac{d\sigma}{d\Omega} = (\gamma r_o)^2 \; S^2(T) \; \frac{(1 + \cos^2\phi)}{4} \; \frac{(2\pi)^3 N}{V_o} \sum_\tau \left[\left(B_o + \frac{B_2}{2} \right)^2 \delta(\kappa - \tau \pm k_o) \right.$$

$$+ \frac{(B_2 + B_4)^2}{4} \delta(\kappa - \tau \pm 3k_o) + \frac{(B_4 + B_6)^2}{4}$$

$$\left. \delta(\kappa - \tau \pm 5k_o) + \frac{B_6^2}{4} \delta(\kappa - \tau \pm 7k_o) \right] \qquad (1.38)$$

where $\vec{\tau}$ is a reciprocal lattice vector and S(T) is the temperature dependent magnetic spin in the basal plane.

From this formulation the form factors for the first and third order satellites are separated and easily calculated using the Stassis et al.[1] tabulated multipoles. It is interesting to note the anisotropy that arises from the calculation (see Figure 1.6). The square of the form factor of the first order satellite, $(B_0 + \frac{B_2}{2})^2$ normalized to 1 in the forward direction, is shown in the figure. The average ϕ form factor is obtained by averaging the sine functions between 0 and $\frac{\pi}{2}$.

Note that the calculated third, fifth and seventh order satellites are due to the higher order multipoles, T_3^m, T_5^m and T_7^m, which appear in the form factor. This deviation from sphericity of the magnetic moment gives rise to a weak modulation of the spin spiral structure.

Now if the spiral structure deviates from purely sinusoidal and the moment's magnitude and direction "bunch" around the easy hexagonal axis (see Figure 1.7) an additional six fold modulation is introduced. This spiral modulation gives rise to fifth and seventh order satellites of much greater intensity than those predicted by the ionic magnetization density asphericity. The turn angle of the spiral becomes modulated and can be written

$$\phi_L = \phi_L^{\circ} + \gamma \sin 6\phi_L + i \frac{\Delta\mu}{\mu} \cos 6\phi_L \ . \qquad (1.39)$$

ϕ_L° is the turn angle of the purely sinusoidal spiral and is measured relative to the hard hexagonal axis. The second term on the right hand side of equation (1.39) describes the moment <u>direction</u> modulation (modulation of turn angle) whereas the third term is imaginary

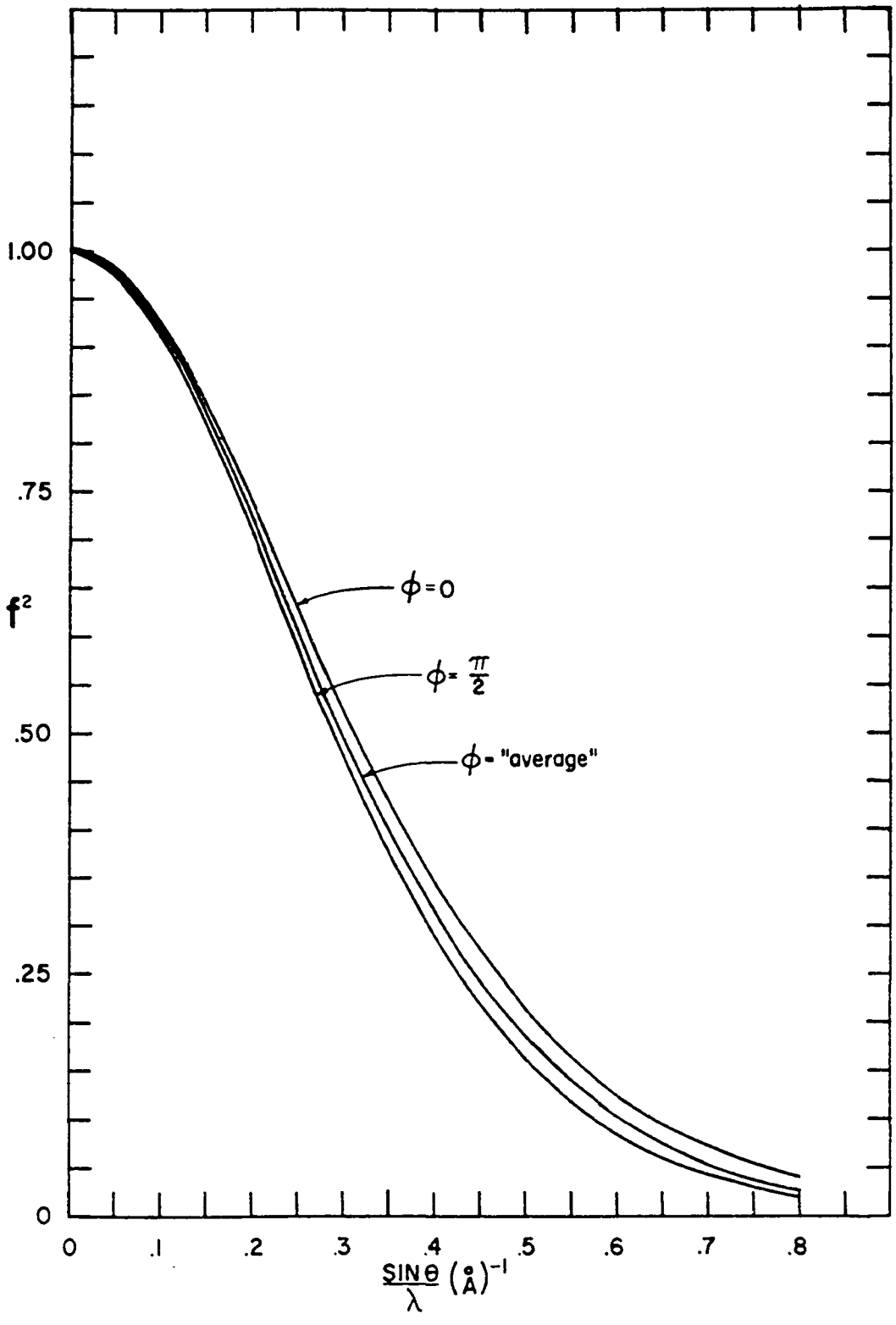

Figure 1.6. First order form factor asymmetry

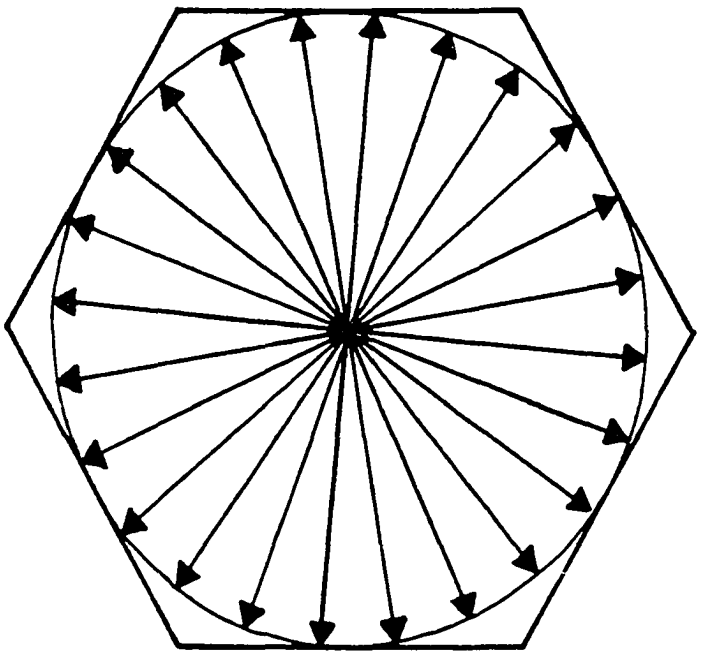

T > 50 K

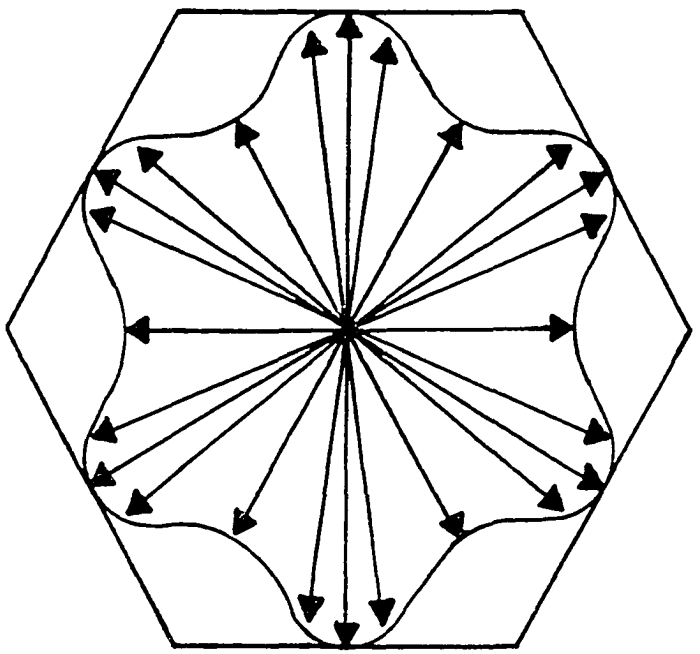

T < 50 K

Figure 1.7. "Bunched" moments

and describes the moment magnitude modulation. Now $e^{i\phi_L}$ becomes

$$e^{i\phi_L} = e^{i\phi_L^o}\,[e^{i\gamma \sin 6\phi_L^o}][e^{-\frac{\Delta\mu}{\mu}\cos 6\phi_L^o}] \; . \tag{1.40}$$

One can expand

$$e^x = 1 + X + \frac{x^2}{2} + \ldots \simeq 1 + X, \text{ for small } x. \tag{1.41}$$

Therefore one can write

$$e^{i\phi_L} = e^{i\phi_L}\,[1 + i\gamma \sin 6\phi_L^o][1 - \frac{\Delta\mu}{\mu}\cos 6\phi_L^o] \; , \tag{1.42}$$

$$= e^{i\phi_L^o} - \frac{1}{2}\,(\gamma + \frac{\Delta\mu}{\mu})\,e^{-i5\phi_L^o} + \frac{1}{2}\,(\gamma - \frac{\Delta\mu}{\mu})\,e^{i7\phi_L^o} \; , \tag{1.43}$$

since

$$\sin x = \frac{1}{2i}\,(e^{ix} - e^{-ix}) \text{ and } \cos x = \frac{1}{2}\,(e^{ix} + e^{-ix}) \; . \tag{1.44}$$

Let $\phi_L^o = \vec{k}_o\vec{R}_j$ and recall equation (1.33) to write

$$\begin{aligned}\vec{S}_j = {} & \frac{S}{2}\,(e^{i\vec{k}_o\cdot\vec{R}_j}\,\hat{m}^+ + e^{-i\vec{k}_o\cdot\vec{R}_j}\,\hat{m}^-) \\ & - \frac{S}{4}\,(\gamma + \frac{\Delta\mu}{\mu})(e^{-i5\vec{k}_o\cdot\vec{R}_j}\,\hat{m}^+ + e^{i5\vec{k}_o\cdot\vec{R}_j}\,\hat{m}^-) \\ & + \frac{S}{4}\,(\gamma - \frac{\Delta\mu}{\mu})(e^{i7\vec{k}_o\cdot\vec{R}_j}\,\hat{m}^+ + e^{-i7\vec{k}_o\cdot\vec{R}_j}\,\hat{m}^-) \; .\end{aligned} \tag{1.45}$$

The sum over α and β becomes

$$\begin{aligned}\sum_{\alpha,\beta}\,(\delta_{\alpha\beta} - \hat{\kappa}_\alpha\hat{\kappa}_\beta)\langle S_{j\alpha}S_{j'\beta}\rangle = {} & \frac{1}{4}\,S^2\,(1 + \cos^2\phi)[e^{i\vec{k}_o\cdot(\vec{R}_j-\vec{R}_{j'})} \\ & + e^{-i\vec{k}_o\cdot(\vec{R}_j-\vec{R}_{j'})} + \frac{1}{4}\,(\gamma + \frac{\Delta\mu}{\mu})^2\,(e^{i5\vec{k}_o\cdot(\vec{R}_j-\vec{R}_{j'})} + e^{-i5\vec{k}_o\cdot(\vec{R}_j-\vec{R}_{j'})}) \\ & + \frac{1}{4}\,(\gamma - \frac{\Delta\mu}{\mu})^2\,(e^{i7\vec{k}_o\cdot(\vec{R}_j-\vec{R}_{j'})} + e^{-i7\vec{k}_o\cdot(\vec{R}_j-\vec{R}_{j'})})]\end{aligned} \tag{1.46}$$

where here terms of the form $e^{\pm i\vec{k}_o\cdot(\vec{R}_j+\vec{R}_{j'})}$ have been omitted because the modulations due to the form factor are neglected here and the $e^{\pm i\vec{k}_o\cdot(\vec{R}_j+\vec{R}_{j'})}$ terms will vanish upon summing over all the atoms in the solid. The total scattering cross section becomes

$$\frac{d\sigma}{d\Omega} = (\gamma r_o)^2 \, f^2(\theta) \, S^2(T) \, \frac{(2\pi)^3 N}{V_o} \, \frac{(1 + \cos^2\phi)}{4}$$

$$\times \sum_{\tau} \left[\delta(\kappa - \tau \pm k_o) + \frac{1}{4} \left(\gamma + \frac{\Delta\mu}{\mu}\right)^2 \delta(\kappa - \tau \pm 5k_o) \right.$$

$$\left. + \frac{1}{4} \left(\gamma - \frac{\Delta\mu}{\mu}\right)^2 \delta(\kappa - \tau \pm 7k_o) \right] \qquad (1.47)$$

This theory predicts the existence of fifth and seventh order satellites and also predicts that the fifth will be larger than the seventh.

CHAPTER II. EXPERIMENTAL DETAILS

The Spectrometer

The measurements were performed at the 5 Megawatt Ames Laboratory Research Reactor using a double axis neutron diffractometer which is controlled by a computer (see Figure 2.1). A neutron wavelength, λ, of 1.05Å, with measured $\frac{\lambda}{2}$ contamination of 0.6%, was obtained from the (311) plane of a beryllium monochromator crystal. This beam was collimated to within 30 minutes of arc before incidence upon the sample table. The intensity of the incident beam was monitored by passing the beam through a low efficiency fission chamber. The neutrons reflected from the sample were counted in a high efficiency 5 cm diameter by 35 cm cylinder filled with BF_3 gas at $\frac{1}{2}$ atmosphere. The wavelength and direction of the incident beam were measured by scanning the detector (2θ scan) through the (111) and (200) peaks of NaCl powder on both sides of the incident beam direction (see Figure 2.2). The angular reproducibility of the spectrometer is $\pm.01^{o}$.

The Sample

A boule containing three large, high purity (see Table 2.1) single crystals of metallic holmium was prepared by B. Beaudry of Ames Lab. The boule was examined with neutrons to determine the crystal with the most favorable orientation, then this crystal was removed from the rest of the boule by spark cutting. This large single crystal was then oriented, to within ±2 minutes of arc. A slice from which the pillar used in the structure measurements was to be extracted, was removed by spark cutting. Several slices suitable for polarized neutron work were also removed.

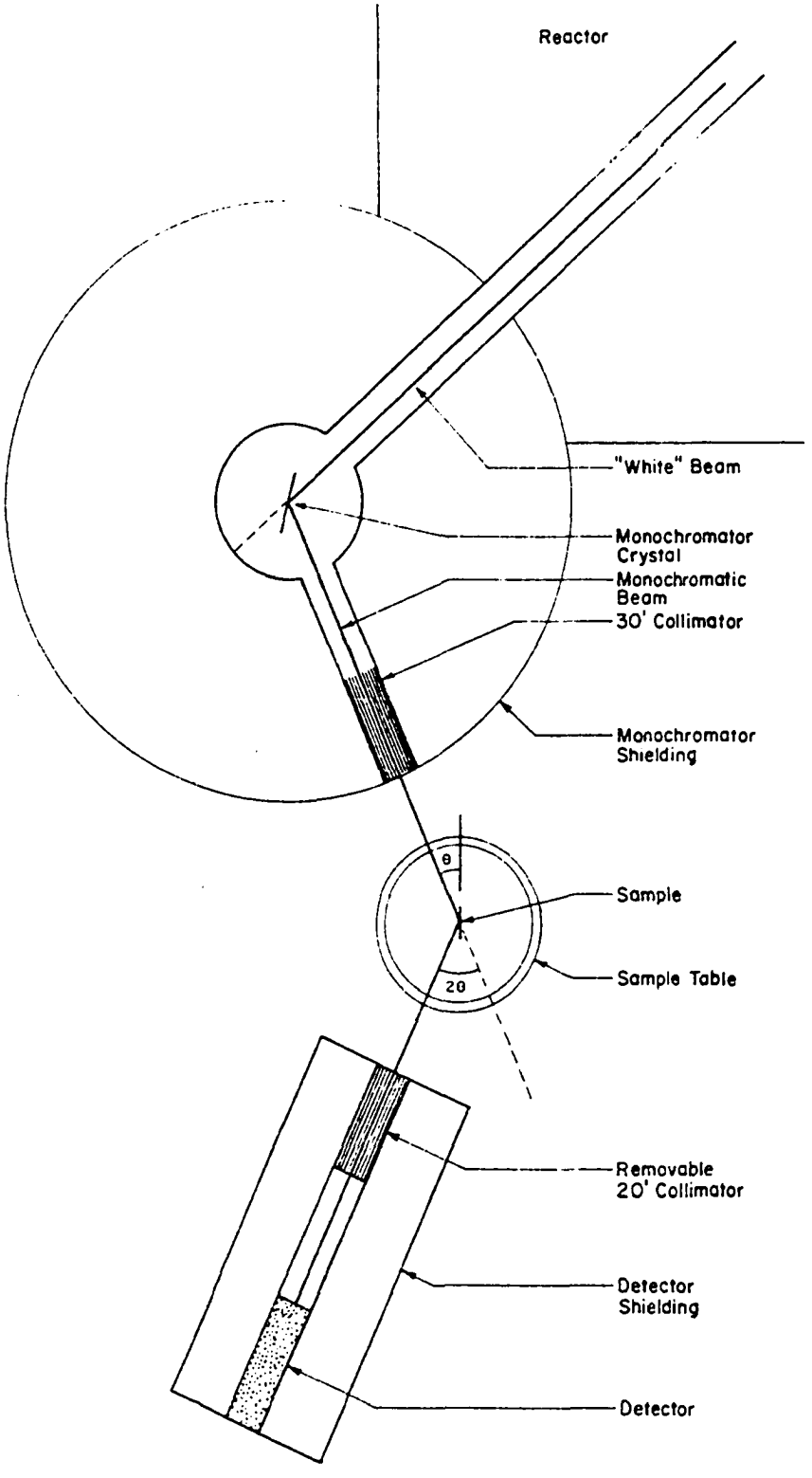

Figure 2.1. Spectrometer

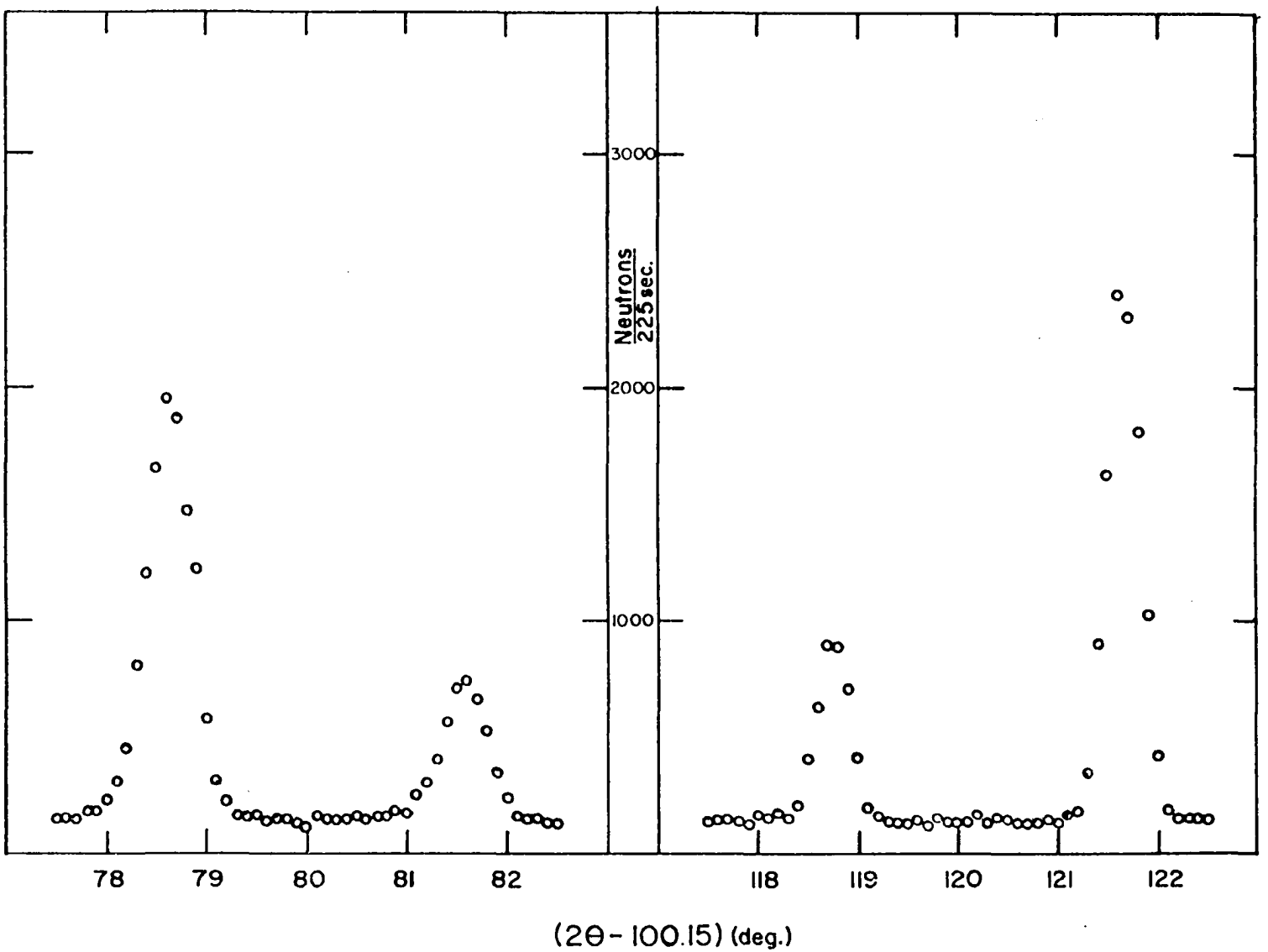

Figure 2.2. NaCl powder scan

Table 2.1. Purity Analysis

Spark Source Mass Spectrometer
Spark Source Mass Spectrometric Analysis-Sample # = HO-111174

LI	BE <.04	B .02	NA .6	MG <.05	AL .3	SI 1	P <.03
S <2	CL 5	K 8	CA .2	TI <.2	V <.02	CR 1	MN <1
FE 30	CO <.06	NI 10	CU 10	ZN .2	GA <.05	GE <.3	AS <.04
SE <.1	KR <.8	RB <.07	SR <.2	ZR <1	NB <1	MO <1	RU <.6
RH <.1	PD <.2	AG <.03	CD <.06	IN <.03	SN <.1	SB <.04	TE .2
I <.04	CS <.004	BA <.08	HF <2	TA 20	W 10	RE <.8	OS <.6
IR <.3	PT <.4	AU .1	HG <.2	TL <.1	PB .6	BI <.05	TH 2
							U <.2

Rare Earth Impurities

SC .6	Y 8.9	LA 1.2	CE 1.2	PR 2.2	ND <2	SM <.2	EU <.2
GD 12	TB <.3	DY <.6	HO	ER <3	TM <.2	YB <.2	LU .60

Vacuum Fusion Results

O 237(23)	N 35(3)	H 327(2)	C 123(9)	F 26(3)	FE 32(11)	NI 11(4)	CU 9(3)

Wt ppm in parentheses

Intensity measurements performed with single crystals must be corrected for secondary extinction effects. In the case of holmium where the intensities of the various nuclear and magnetic diffraction peaks differ by several orders of magnitude, the correction for secondary extinction effects may introduce a considerable uncertainty in the calculated moments. Therefore rather than correcting for extinction we will prepare the sample in such a way that secondary extinction is not a problem.

Secondary extinction arises because the microscopic mosaic blocks (~1000Å on a side) which comprise a macroscopic single crystal are so well-oriented (small mosaic spread) with respect to one another that the neutron beam becomes appreciably attenuated as it passes through the sample -- the stronger reflecting planes of the crystal attenuating the beam more than the weaker reflecting planes. This results in the volume of the sample not being uniformly bathed in the neutron beam in reflections from one plane of atoms relative to another plane. If one can make sure that even the strongest reflection is not being appreciably attenuated, then of course the weaker reflections are not being attenuated and sample volume effects can be eliminated from the data analysis. The attenuation effect on the neutron beam is decreased as the mosaic width of the sample is increased. An increase in mosaic width can be brought about by compression or by suddenly cooling the sample. The former process allows for much greater control.

The full width at half maximum (FWHM = 2.36 x mosaic width) necessary for a sample of a given thickness (neutron path length) to be free of secondary extinction is calculated as follows. The sample is free of

extinction if

$$\frac{\alpha}{\eta} < \frac{1}{4} \tag{2.1}$$

where

$$\eta = \text{mosaic width} = \frac{\text{FWHM}}{2.36} ,$$

$$\alpha = \frac{Qt_o}{\cos\theta} , \text{ (transmission)},$$

$$= \frac{Q\ t_o}{\sin\theta} , \text{ (reflection)}, \tag{2.2}$$

$$Q = \frac{\lambda^3 |F|^2\ N_c^2}{\sin 2\theta} , \tag{2.3}$$

λ is the neutron wavelength, t_o is the sample thickness, N_c is the number of unit cells per unit volume and $|F|^2$ is the structure factor of the particular reflection. Therefore the extinction free condition becomes

$$\text{FWHM} > (2.36)4\ \frac{\lambda^3 F^2 N_c^2 t_o}{\cos\theta\ \sin 2\theta} , \text{ (transmission case)} \tag{2.4}$$

The calculated value of the FWHM for the sample to be used in the structure measurements was 27 minutes of arc. The initial FWHM of that sample slice was measured, by performing a θ scan (sample rotation) in a beam of highly defined wavelength from the (111) plane of a perfect germanium monochrometer, and was determined to be 8 minutes of arc. The sample was then squeezed gently in a machinists vice and the FWHM of the (002) was remeasured. This process was repeated until the FWHM of the (002)

was 30 minutes of arc. From this slice a pillar 1 mm x 1 mm x 1 cm was removed by spark cutting. The pillar was oriented so that the (hol) crystallographic plane was perpendicular to the long axis.

This pillar was then examined at room temperature for secondary extinction effects. To measure for extinction it is necessary to understand the formulation of the structure factor in terms of the measured intensity. The structure factor (F^2) is written

$$CF^2 = \frac{I\sin 2\theta}{e^{-2W}} , \tag{2.5}$$

where

$$W = B \left(\frac{\sin\theta}{\lambda}\right)^2 , \tag{2.6}$$

I is the integrated reflectivity of the reflecting plane, C is a constant of normalization and B is related to the Debye temperature[5] (θ_D). From this we can write

$$\ell n \ \frac{I\sin 2\theta}{F^2} = \ell n \ C - 2B \ \left(\frac{\sin\theta}{\lambda}\right)^2 . \tag{2.7}$$

Therefore if one plots $\ell n \ \frac{I\sin 2\theta}{F^2}$ as a function of $\left(\frac{\sin\theta}{\lambda}\right)^2$ one should obtain a straight line which has a slope of -2B (see Figure 2.3). If the stronger (low $\sin\theta/\lambda$) reflections fall below a straight line the sample suffers from extinction. When measuring for extinction effects no collimation should be used between the sample and the detector as low 2θ reflections are being directly compared with high 2θ reflections and any misalignment of the collimation would cause non-uniform collection of the reflected neutrons. Extinction measurements were made both outside the

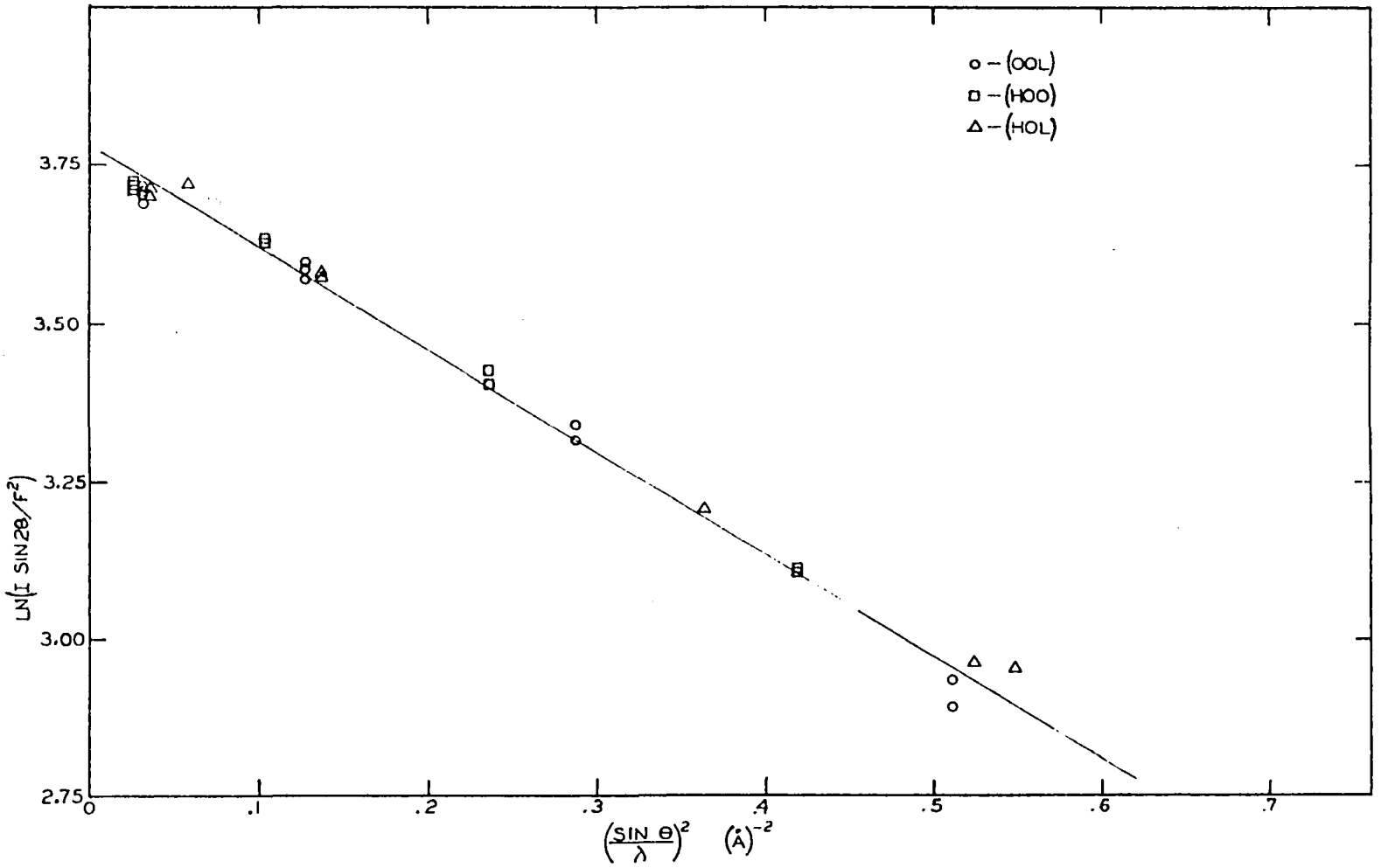

Figure 2.3. Extinction plot

cryostat, for precise θ_D determination, and inside the cryostat to closely simulate experimental conditions. In both cases the pillar was mounted on a goniometer and centered on the sample table by watching the sample through a transit while rotating the sample table. The horizontal translation of the goniometer was adjusted until the pillar did not translate while the sample table was rotating.

The pillar was positioned vertically in the neutron beam by adjusting the goniometer height and the goniometer arcs until the (002) and $(00\bar{2})$ reflections would both center vertically in the detector simply by rotating the sample table by 180^{o}. Each reflection measured was optimized vertically in the counter using the arcs of the goniometer. Then a θ (sample table) scan was performed followed by a 2θ (detector) scan to determine the optimum angular positions of each reflection. These angular positions were optimized to within 0.02^{o}. To measure the intensity of a given reflection a θ-2θ scan was performed about the optimum angular positions. In the θ-2θ scan the sample table half-angles with the detector and the sample is always in a position to Bragg reflect.

The integrated reflectivities of the (100), (200), (300), (400), (002), (004), (006), (008), (101), and (202) were measured and to within experimental error the results were consistent with negligible secondary extinction and a Debye temperature of 159±3K.

The Magnetic Measurements

The holmium sample was mounted in a cryostat which, in turn, was placed on a goniometer and the entire assembly mounted on the spectrometer sample table. The sample was positioned in the neutron beam using the

same methods described in the extinction measurement section. For the magnetic measurements a 20' collimator was positioned between the sample and the detector, in order to be able to separate the magnetic satellites from the nuclear peaks at lower temperatures (see Figure 2.4). The collimator does not appreciably affect the magnetic measurements because all magnetic satellite reflections are normalized to their respective nuclear reflections, and these are relatively close to one another in detector angle (2θ). In measuring the (300) and (008) reflections the primary concern is angular position rather than intensity and the collimation allows much greater 2θ position resolution.

The temperature of the sample was controlled to within $\pm\frac{1}{2}^{o}$K by a Cu vs. constantan thermocouple above 50K and by a Cu vs. Au-Fe (3%) thermocouple below 50K. Control of the temperature was provided by a potentiometer set to balance the emf generated by the thermocouple at a given temperature. This balance was indicated on a null detector which switched the sample heater on and off as it passed through the zero point. Liquid nitrogen and liquid helium were used to cool the sample. An electrical resistance heater was wound around a copper block, located between the sample and the inner liquid container, to heat the sample above 6K and 77K (see Figure 2.5).

At each temperature the following steps were made:

1) Center the (300) and (008) vertically in the detector with the goniometer arcs to bring the (hol) plane of the sample into coincidence with the scattering plane.

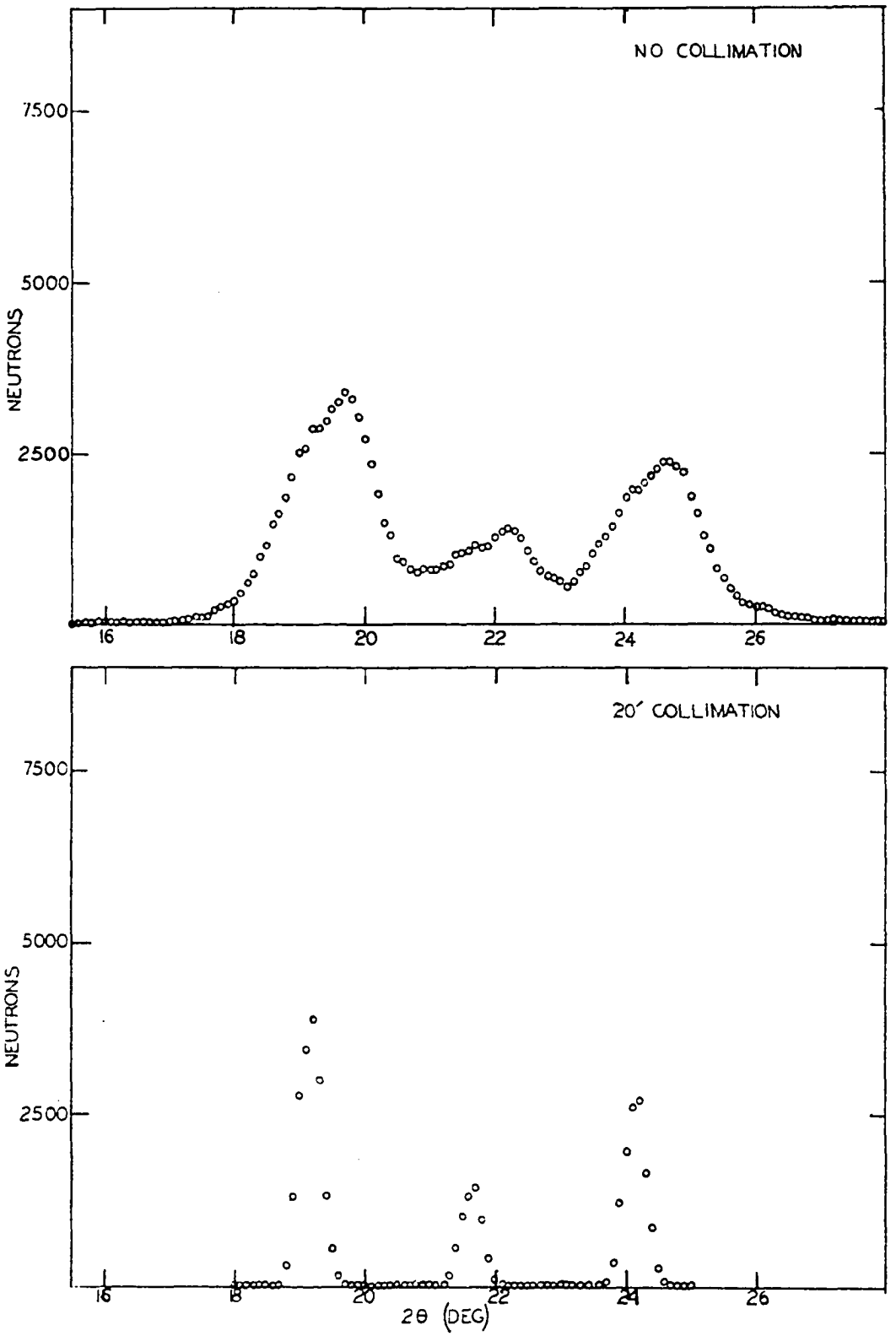

Figure 2.4. Scan around (002) with and without collimation

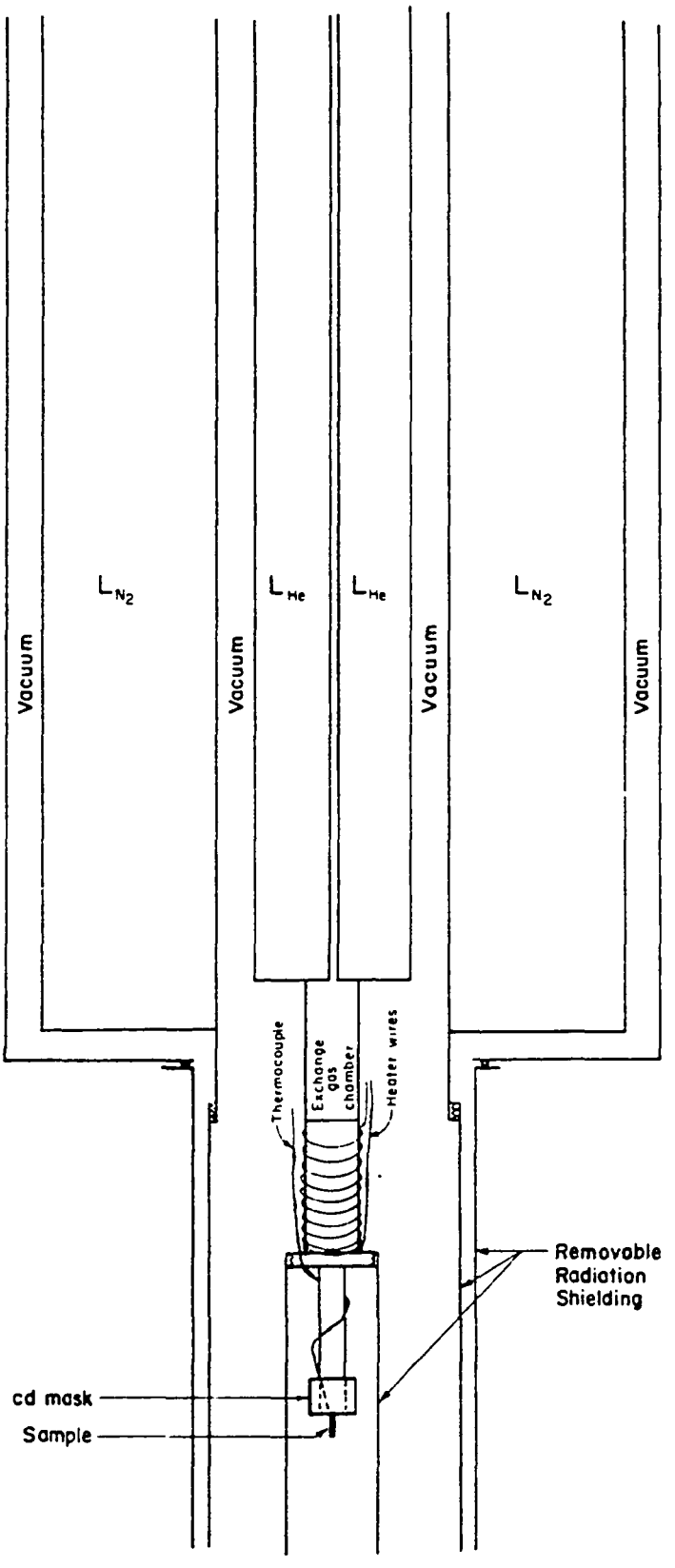

Figure 2.5. Cryostat

2) Double rock (θ scan then θ-2θ scan) (300) and (008) to determine the lattice constants a and c, and thereby determine the reciprocal space associated with the chemical unit cell.

3) Perform a q_z scan around the (101) in the [00ℓ] direction, measuring the center of gravities of the $(101)^{\pm 1}$ magnetic reflections to determine the magnetic periodicity (a computer program allows a scan to be made along any straight line in q space) (see Figure 2.6).

4) Combine the reciprocal space and magnetic periodicity information to predict, with the use of the computer, the positions of magnetic satellites and nuclear peaks.

5) Measure, by θ-2θ scan centered around predicted centers, intensities of (100), $(100)^{+}$, (101), $(101)^{\pm}$, (002), and $(002)^{\pm}$.

6) Analyze intensity by measuring the area above background, of the θ-2θ scan. The angular position of the reflection was obtained by determining the center of gravity of the scan.

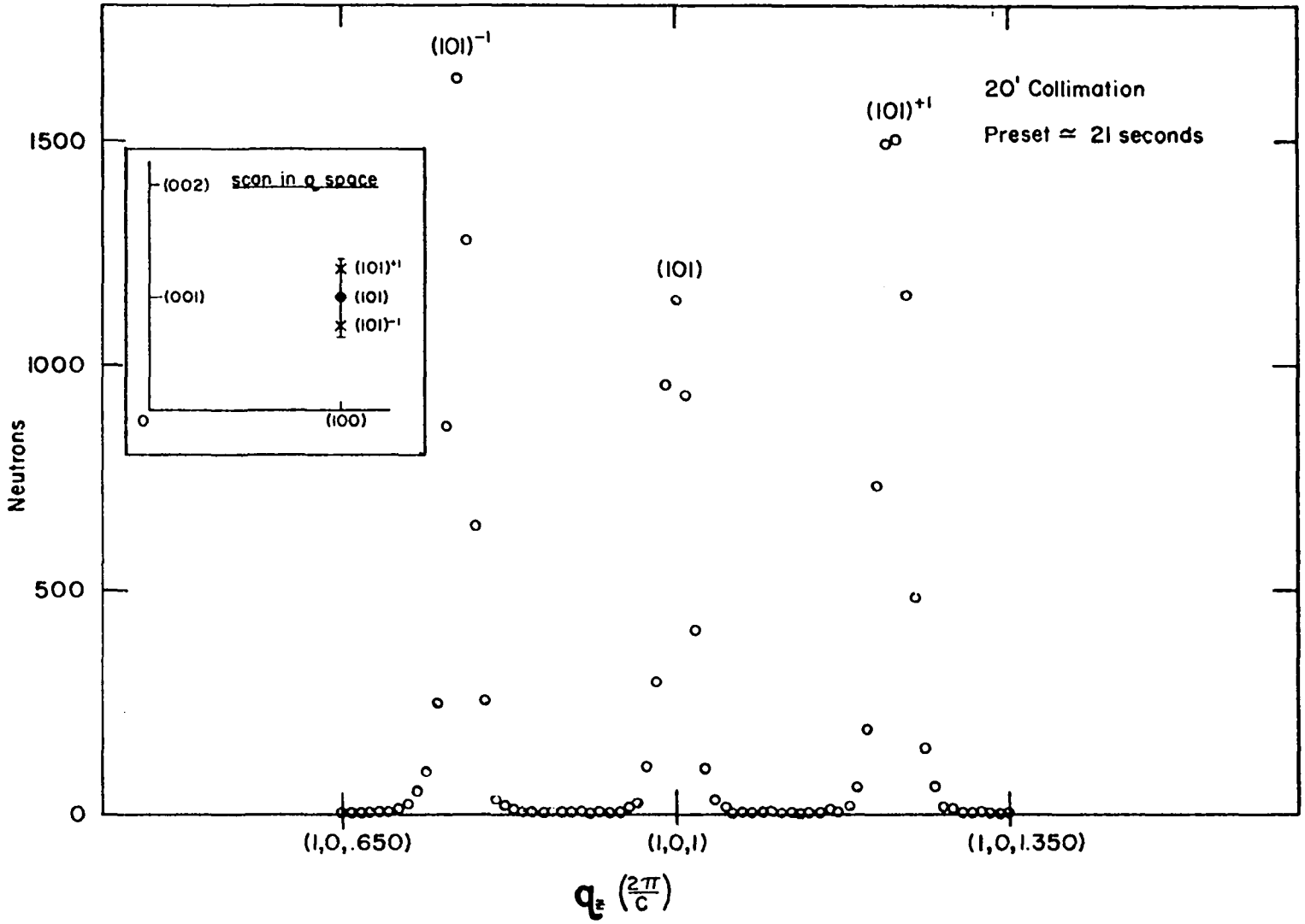

Figure 2.6. q_z scan

CHAPTER III. EXPERIMENTAL RESULTS

Transition Temperatures and the Magnetic Spiral

Below 140K the (00ℓ) plane was monitored between [000] and [001] in search of the $(000)^{+1}$ magnetic satellite. Because this is such a strong reflection it provides a sensitive indication of the formation of the magnetic spiral structure. At 132K the $(000)^{+1}$ reflection was very weak and broad. At 131K this magnetic reflection had become clearly evident and its full width at half maximum (FWHM) was equal to the FWHM observed for the nuclear reflections. Below 131.5 ± .5K the basal plane moment of holmium orders in a purely sinusoidal antiferromagnetic spiral with wave vector (2π divided by the periodicity) along the c axis. This is evidenced by the observations of only first order satellites at $\pm k_o$ (see relation 1.34) around each nuclear reflection. The temperature dependence of several reflections is given in Figures 3.1, 3.2, and 3.3.

Below 77K magnetic satellites were observed around the (300), and other nuclear reflections at $\pm 3k_o$. These third order magnetic satellites arise from the higher order multipoles in the ionic magnetization density.

Below 50K magnetic satellites were observed between (000) and (002) at $\pm 5k_o$ and $\pm 7k_o$. These fifth and seventh order satellites are evidence that the spiral structure deviates from a purely sinusoidal periodicity.

Below 20K an increase in intensities of the (100) and (101) nuclear reflections is observed. The (002), however, showed no increase in intensity. These observations are characteristic of a ferromagnetic component appearing along the c axis. This component reached its full value of 1.6 μ_B at 6K.

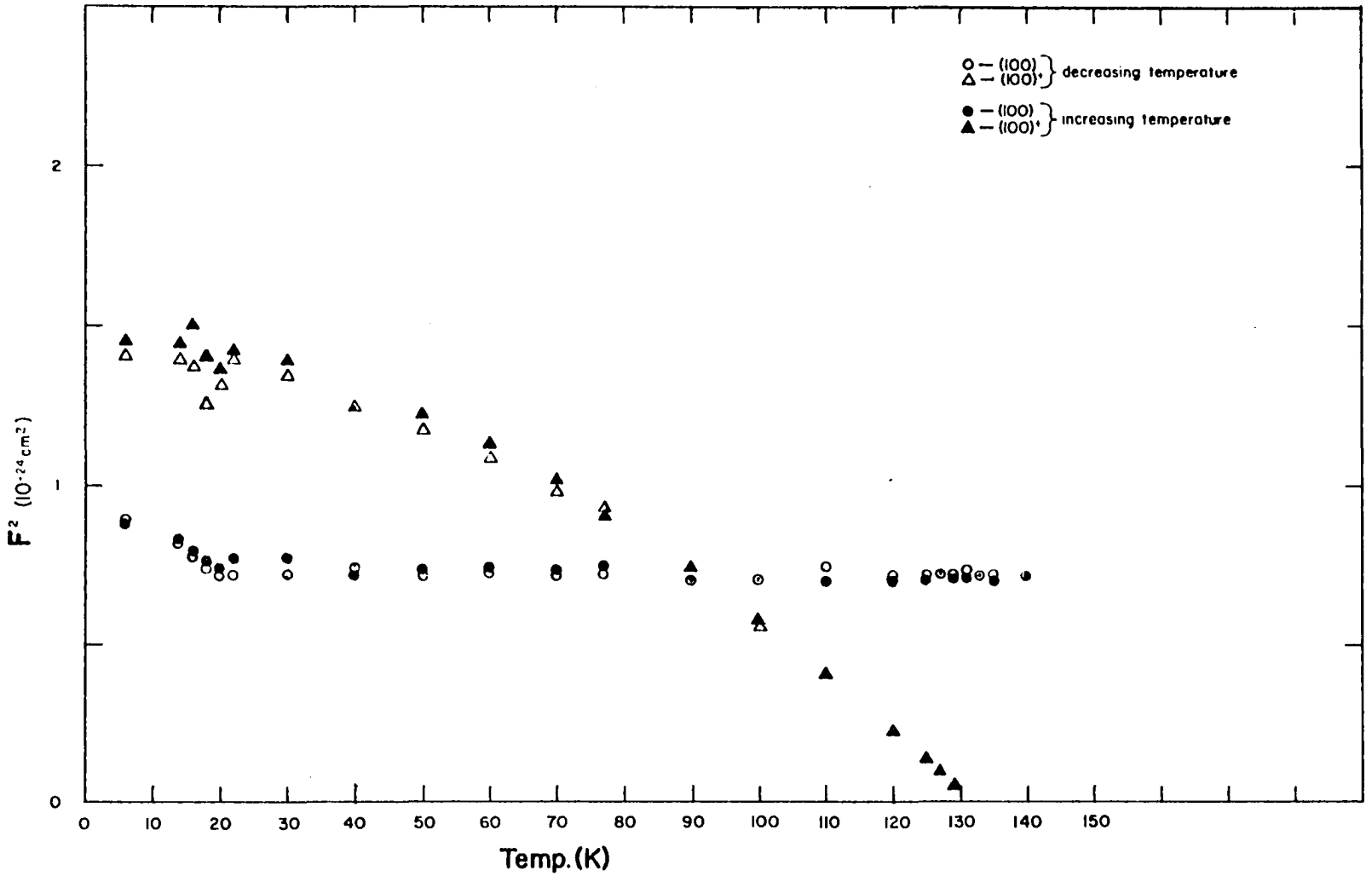

Figure 3.1. Structure factor of the (100) and $(100)^+$ vs. temperature

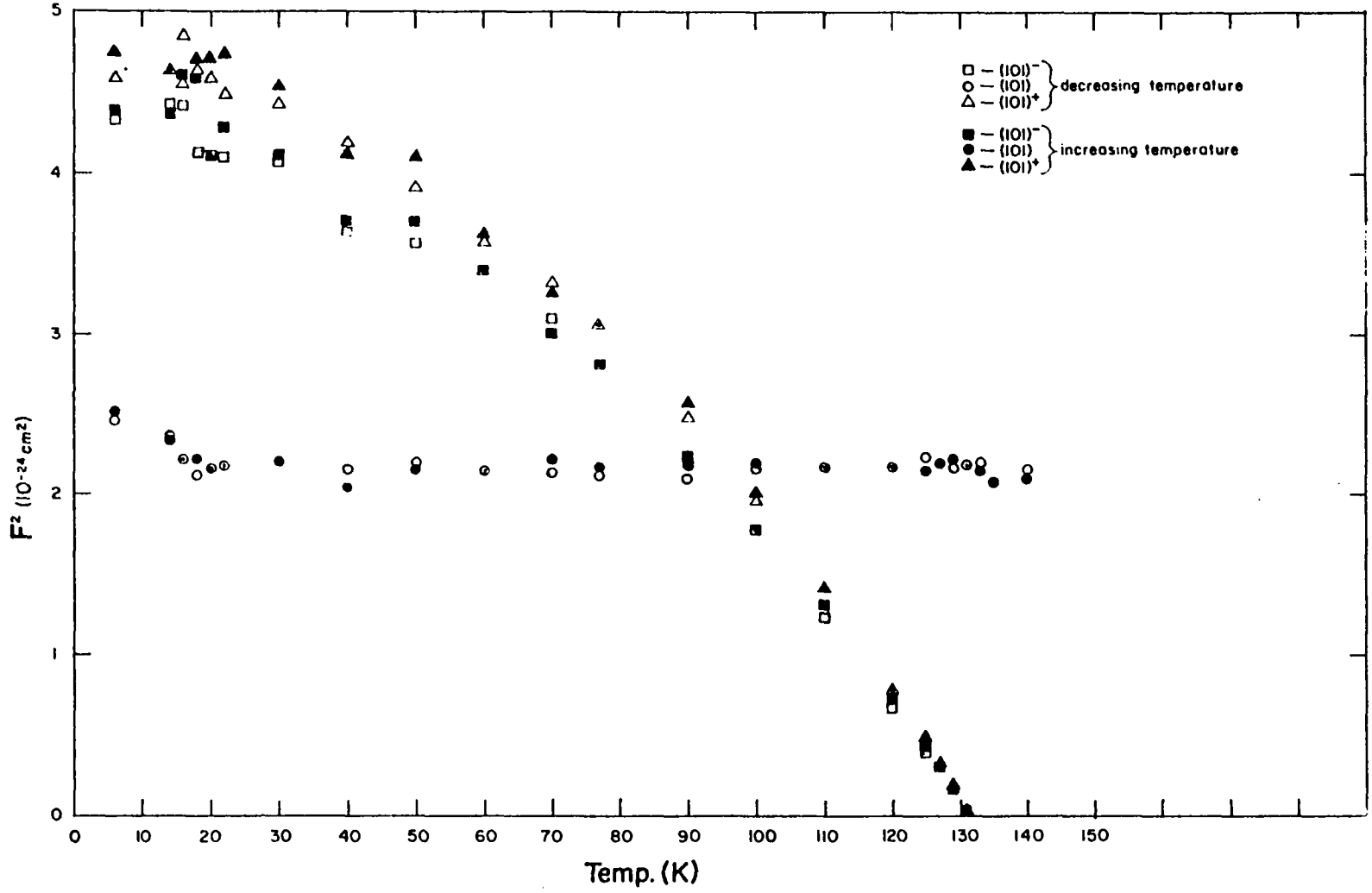

Figure 3.2. Structure factor of the (101) and $(101)^{\pm}$ vs. temperature

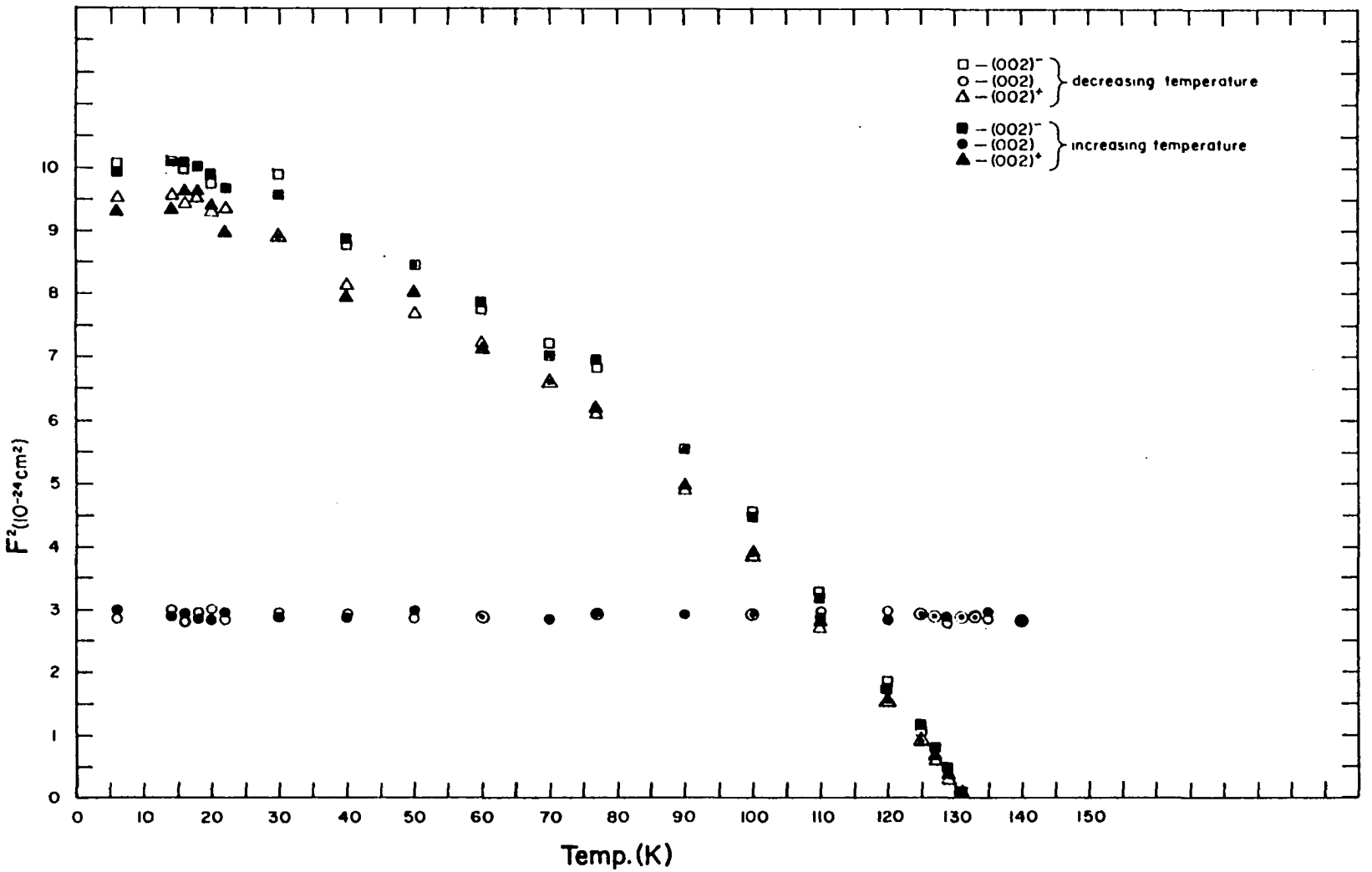

Figure 3.3. Structure factor of the (002) and $(002)^{\pm}$ vs. temperature

Temperature Variation of the Magnetic Periodicity

The wave vector of the magnetic spiral is .279 $(\frac{2\pi}{c})$ at 131K and decreases monotonically to a value of .185 $(\frac{2\pi}{c})$ at 22K (see Figure 3.4). Between 22K and 16K the wave vector decreases more sharply to a value of .168 and remains constant as the temperature is decreased to 6K. The measurements were performed during warming as well as cooling of the sample and a slight hysteresis effect was observed around the Curie temperature.

The temperature dependence of the wave vector shows several inflections where the curvature of the function changes sign. These inflections occur, roughly, where the magnetic unit cell is commensurate with 4, 5, and 6 times the chemical unit cell.

Magnetostriction

The temperature variation of the lattice constants, determined from the measured (300) and (008) scattering angles, is given in Figure 3.5. Above 131K the lattice constants $\underline{a}$ and $\underline{c}$ both decrease, $\underline{c}$ decreasing more rapidly than $\underline{a}$, and the sample contracts. Between 131K and 20K the effects of magnetic ordering are apparent. The $\underline{c}$ axis is stretched out at the expense of the $\underline{a}$ axis. Below 20K $\underline{c}$ and $\underline{a}$ are constant. Below T_N the volume of the unit cell decreases very slowly as the temperature is lowered,

$$\left(\frac{\partial V}{\partial T}\right)_{T<T_N} < \left(\frac{\partial V}{\partial T}\right)_{T>T_N} \quad \text{(see Figure 3.6).} \qquad (3.1)$$

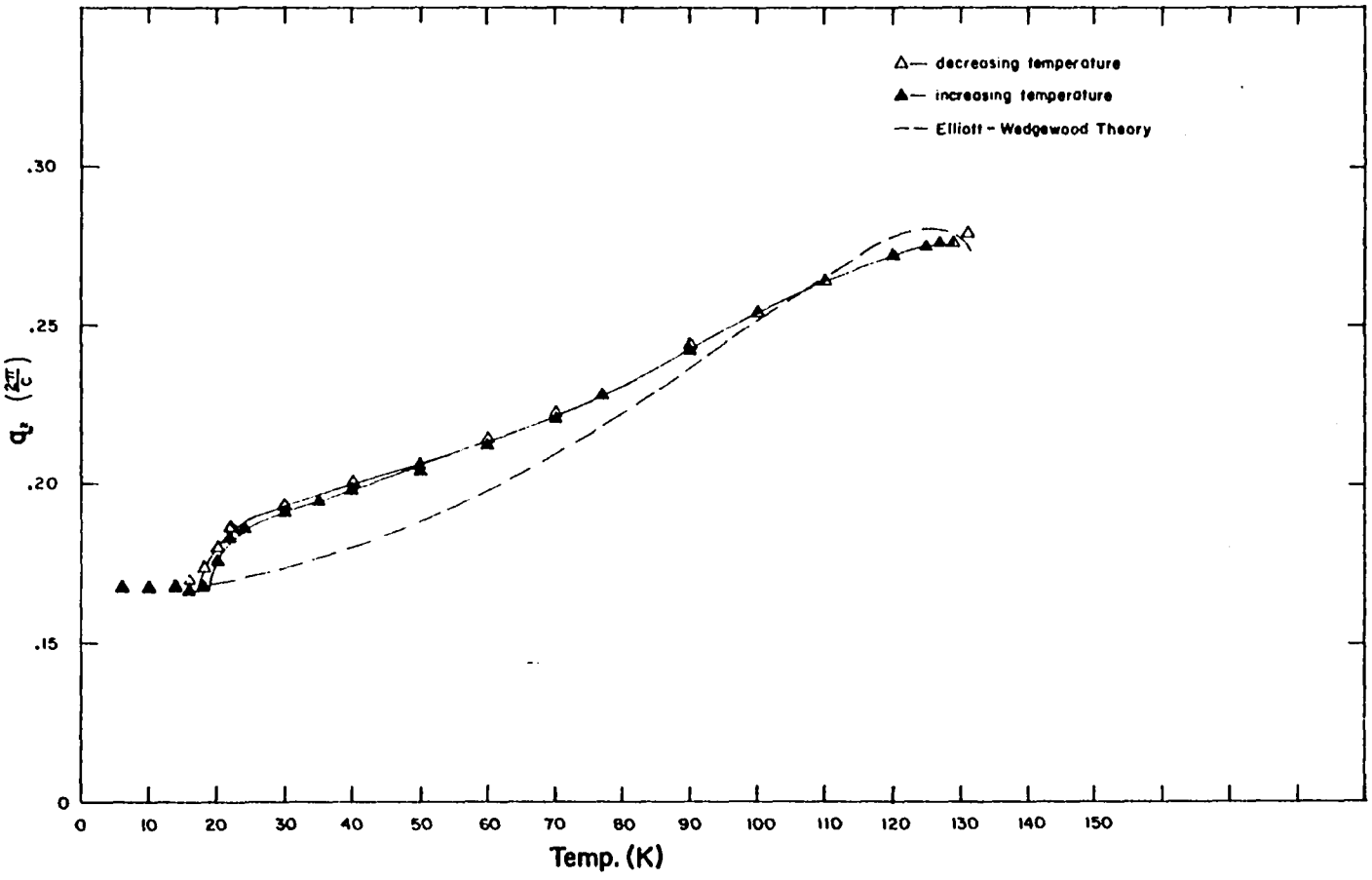

Figure 3.4. Magnetic periodicity vs. temperature

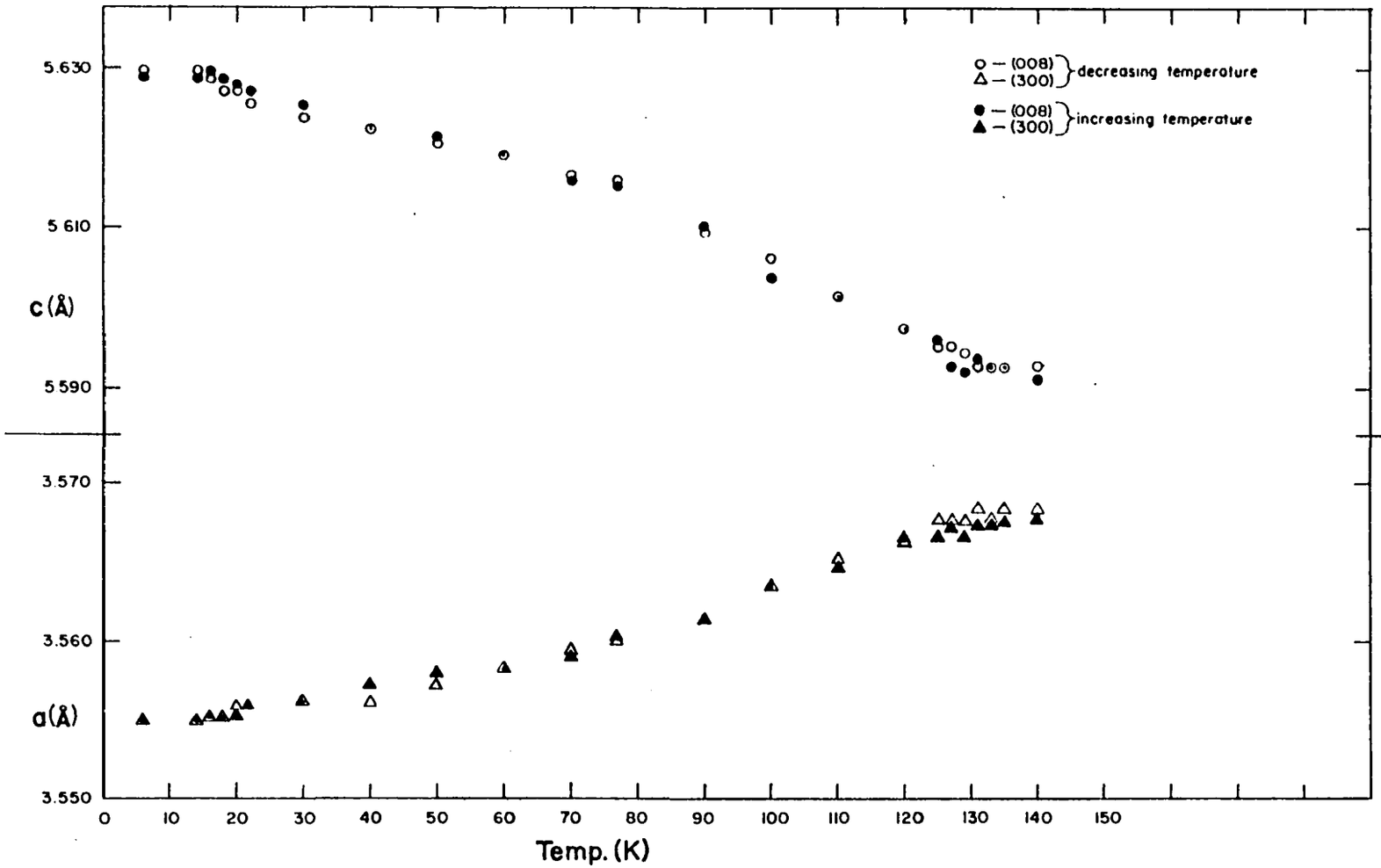

Figure 3.5. Lattice parameters vs. temperature

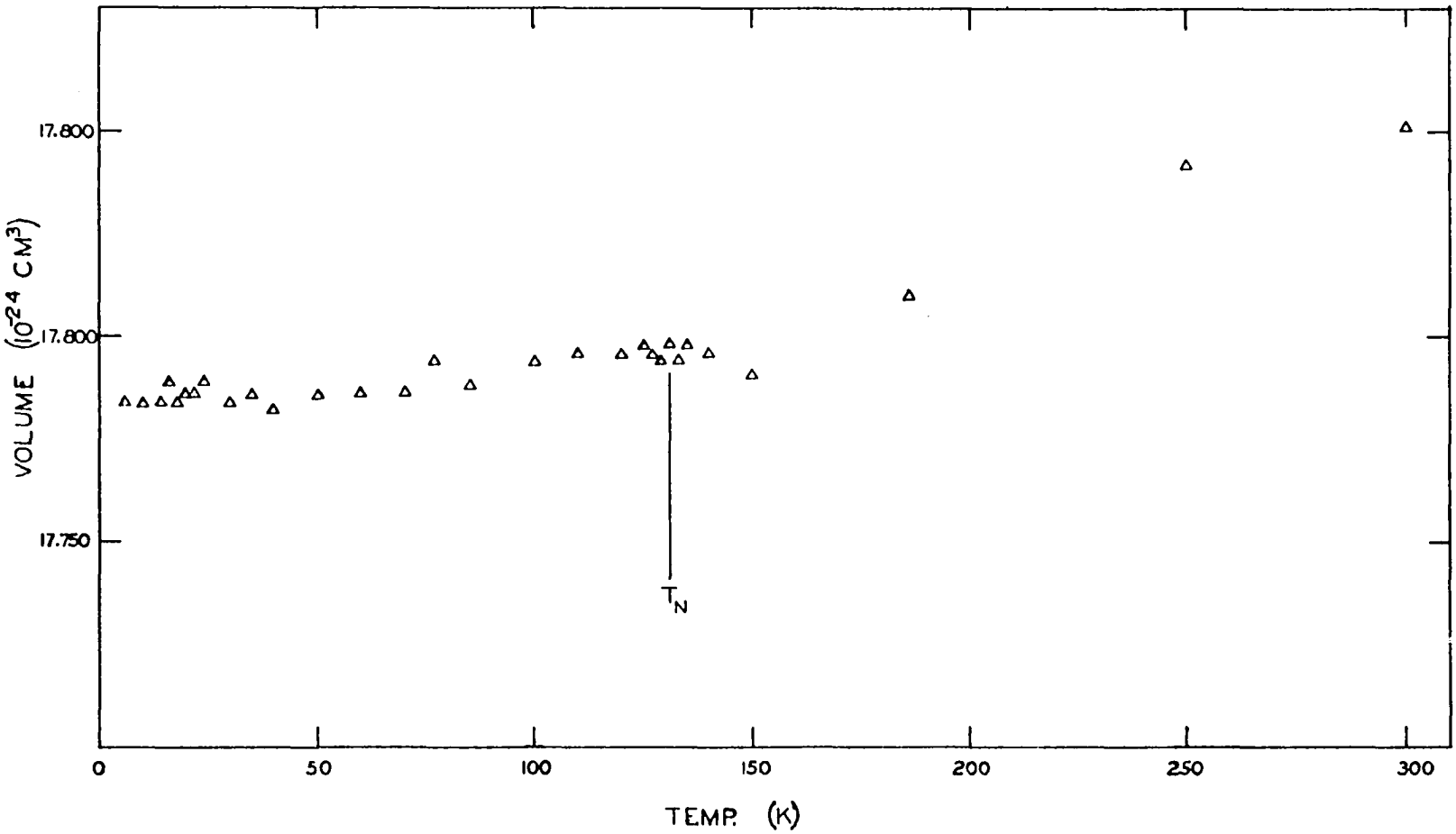

Figure 3.6. Volume of the unit cell vs. temperature

Magnetic Moments

The magnetic moment is obtained from the measured magnetic, and corresponding nuclear, intensities (see equation 2.5) as follows. Write the square of the structure factor for the n^{th} order satellites as

$$F^2_{(hk\ell)}{}^{\pm n} = P_o{}^2 \frac{(1 + \cos^2\phi)}{4} \mu^{2n} f^2 G^2_{(hk\ell)} \tag{3.2}$$

where $P_o{}^2 = 0.0725$ and μ is the moment in the basal plane expressed in Bohr magnetons, f^2 is the atomic magnetic form factor, ϕ is the angle between the scattering vector and the $\underline{c}$ axis and $G^2_{(hk\ell)}$ is the geometrical structure factor. Now

$$G^2_{hk\ell} = \frac{F^2_{hk\ell}}{b^2} \quad \text{(from the nuclear reflections)}, \tag{3.3}$$

therefore the magnetic moment can be expressed as

$$\mu_n = \frac{4b^2 F^2_{(hk\ell)}{}^{\pm n}/F^2_{(hk\ell)}}{P_o{}^2 (1 + \cos^2\phi) f^2}^{\frac{1}{2}} . \tag{3.4}$$

The ferromagnetic component, observed along the c axis below T_c, is analyzed as follows

$$F^2_{(hk\ell)m} = P_o{}^2 \mu^2 f^2 G^2_{(hk\ell)} q^2 , \tag{3.5}$$

where $q = \sin\phi$, ϕ is the angle between the scattering vector and the moment ($\underline{c}$ axis in this case) and μ is the component of the magnetic moment parallel to the $\underline{c}$ axis. Again substitute for $G^2_{(hk\ell)}$ and obtain

$$\mu = \frac{b^2 F^2_{(hk\ell)m}/F^2_{(hk\ell)}}{P_o{}^2 f^2 \sin^2\phi} . \tag{3.6}$$

The form factor, f^2, used in calculating these moments was obtained from the Koehler et al. Ho_2O_3 paramagnetic measurements[6]. This form factor, by the way, agreed very well with the Stassis-Deckman based form factor calculated elsewhere in the paper. In analyzing the data a value $b = 0.85 \times 10^{-12}$ cm for the coherent nuclear scattering amplitude was used.

The magnitude of the moment giving rise to the first order satellite is shown as a function of temperature in Figure 3.7. The moment begins ordering in the basal plane at 131.5K. Below approximately 100K the $(100)^{+1}$ magnetic moment becomes larger than the $(101)^{\pm}$ moment which is in turn larger than the $(002)^{\pm}$ moment, until at 6K the $(100)^{+}$ moment is 0.4 μ_B larger than the $(002)^{\pm}$ moment. Note also that through the Curie temperature the $(100)^{+}$ moment drops from 9.8 to 9.3 ($\pm$0.1) μ_B and then returns to 9.8 μ_B. These observations below 100K are consistent with the existence of a small (.4 μ_B at 6K) $\underline{c}$ axis moment which is modulated with the same periodicity as the basal plane moment. As the structure goes from the helical to the conical structure at T_c this $\underline{c}$ axis modulation is disturbed momentarily. After passing through the transformation the c axis modulation returns to its previous state and we have a ferromagnetic moment along the $\underline{c}$ axis which oscillates in magnitude (type of ferrimagnetism).

Below 50K the spiral begins to deviate from a purely sinusoidal periodicity. In each ferromagnetic layer the moments have a tendency to "bunch" around the easy hexagonal axis. This produces a six-fold modulation of the periodicity and gives rise to fifth and seventh order satellites. It is also observed that the (00ℓ) fifth order satellite

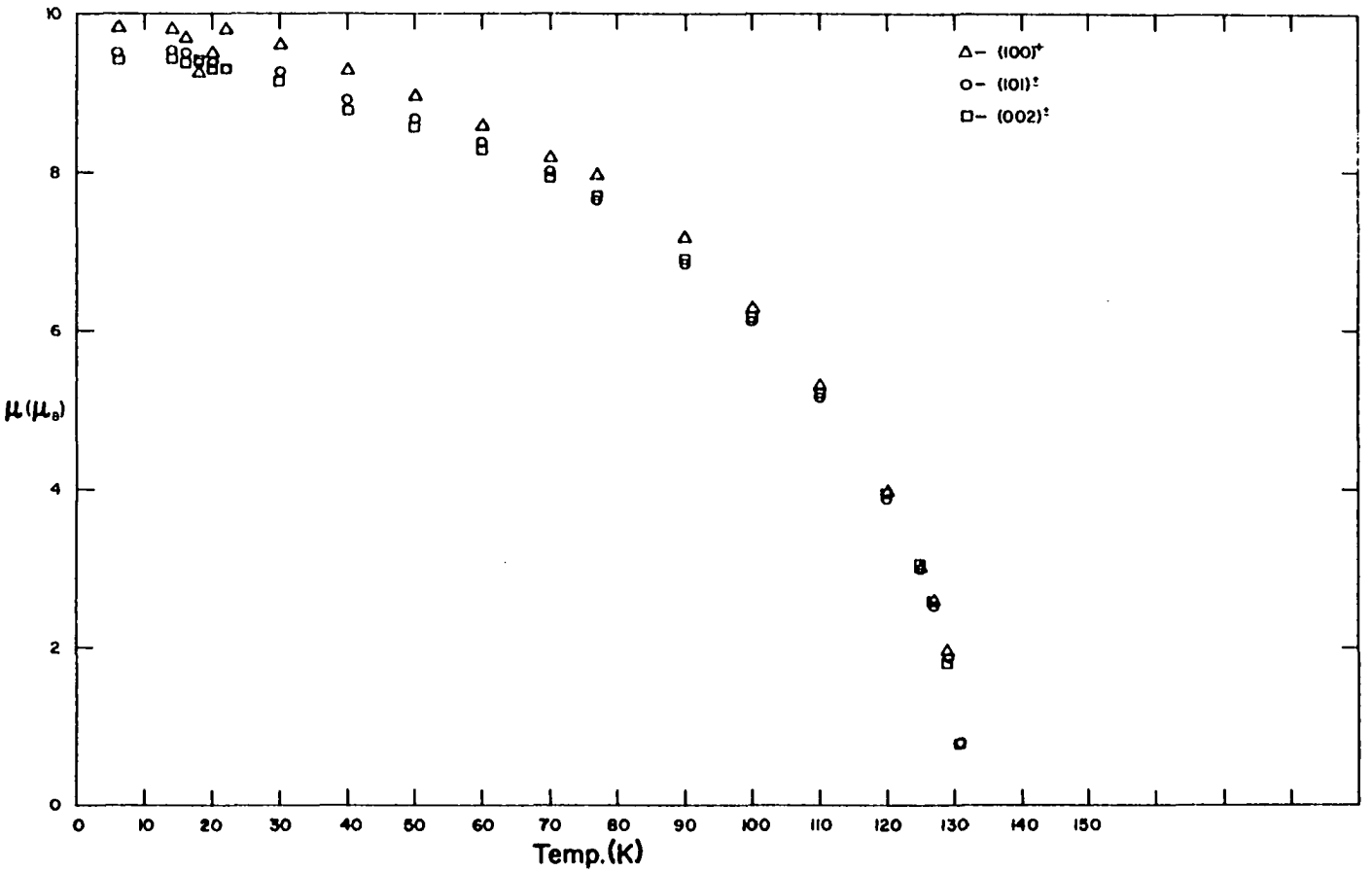

Figure 3.7. Magnetic moments vs. temperature

has approximately 2.5 times the structure factor that the seventh order satellite has. (This is also true of the (300) fifth and seventh order satellites.) This indicates that not only is the direction of the moment modulated but the magnitude of the moment is less along the hard hexagonal directions.

It is seen in figure (3.8) that the difference in the magnetic moment between the fifth and seventh order satellite at T = 22K is $\Delta\mu = .28\ \mu_B$. This value of $\frac{\Delta\mu}{\mu} = .03$ and the relations

$$\mu_5 = \frac{\mu_0}{2}\left(\gamma + \frac{\Delta\mu}{\mu}\right) \tag{3.7}$$

and

$$\mu_7 = \frac{\mu_0}{2}\left(\gamma - \frac{\Delta\mu}{\mu}\right) \tag{3.8}$$

show measured results to be consistent with $\gamma \simeq .12$ at 22K. This agrees with previous measurements by Felcher et al.[7]

Below 20K the magnetic unit cell became commensurate with chemical unit cell at $K_o = \left(\frac{1}{6}\right)\frac{2\pi}{c}$. Because of this the $(000)^{+5}$ and the $(002)^{-7}$ reflections became superimposed and were not separable. Therefore in order to get an idea of the temperature dependence of the fifth and seventh order satellites throughout their whole range of existence a plot was made of the moment which would give rise to the added intensities of the $(000)^{+5}$ and $(002)^{-7}$. Because of this overlap of the fifth and seventh order satellites there is no way to know if the moment <u>magnitude</u> modulation $\left(\frac{\Delta\mu}{\mu}\right)$ is present below the Curie temperature.

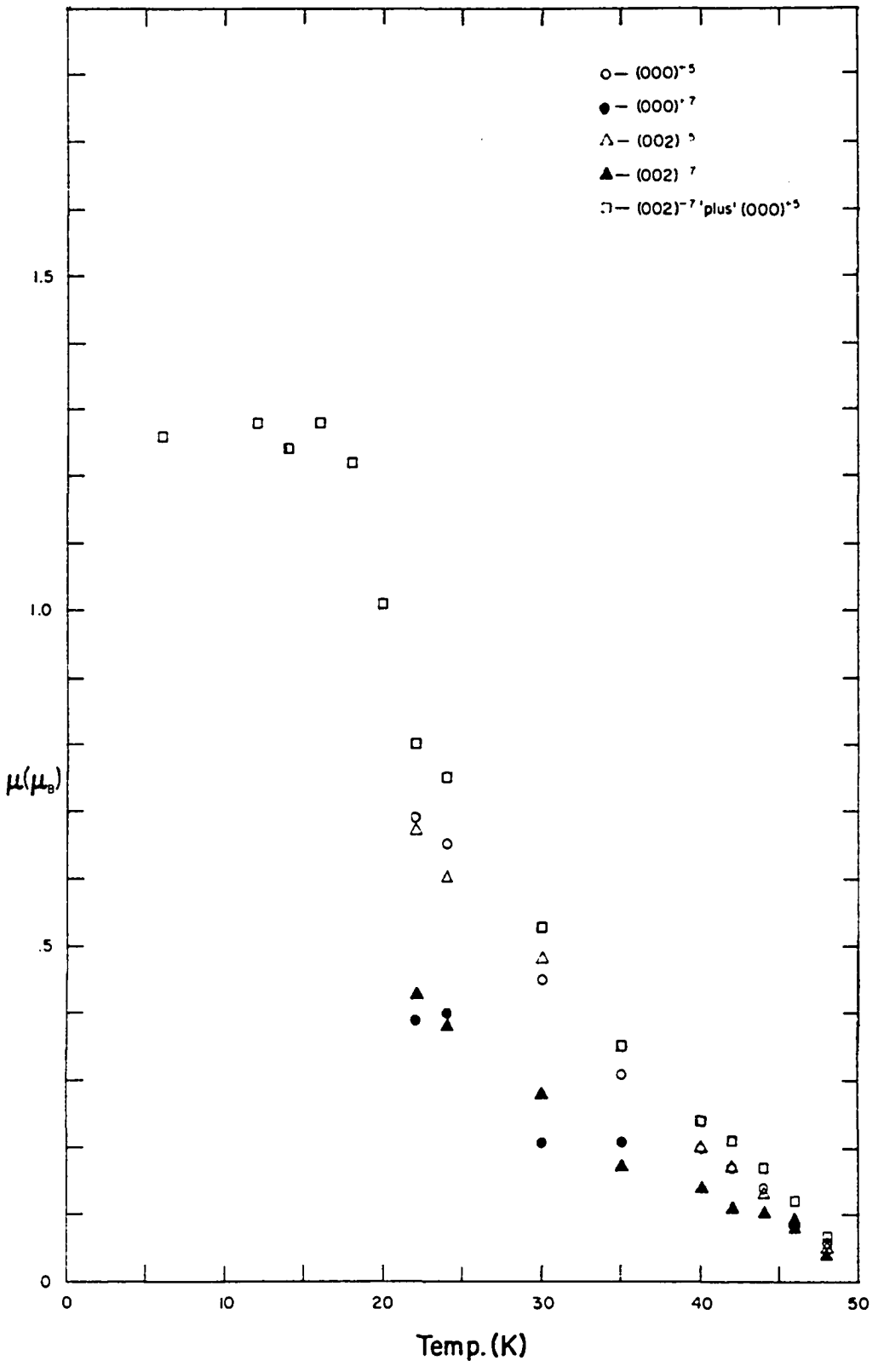

Figure 3.8. Fifth and seventh order moments vs. temperature

Below 80K the higher order multipole contribution to the magnetic moment becomes apparent as is evidenced by the appearance of the third order satellites.

Below 20K the magnetic moment begins to rise out of the basal plane forming a conical structure. The ferro-magnetic component reaches a value of 1.6 μ_B at 6K and the modulated component of the moment reaches a value of 9.8 μ_B at 6K. This gives a total moment of 9.95 μ_B, very close to the saturated value of 10 μ_B found in the free ion.

Magnetic Form Factor

The magnetic form factor of the first order satellites was measured at 77K and 6K (see Figure 3.9). The results are compared with the form factor calculated using the fully relativistic magnetic multipoles tabulated by Stassis et al.[1] The calculated form factor exhibits an asymmetry in the spiral structure which depends upon the angle (ϕ) between the scattering vector and the c axis. The first order data is compared to an averaged form factor using $\langle \sin^{2n}\phi \rangle$ in the expressions for B_{2n} (see equation 1.31).

The data were fit to the calculated form factor using the least squares method.

The third order satellites are extremely weak being 10^{-2} to 10^{-4} of first order intensity. To make measurements of the third order satellites, a sample, 158 times the volume of the pillar in size, was substituted for the pillar. This sample was free of secondary extinction for only the third order satellites and the (300) fifth and seventh order satellites. Therefore the third order satellites from the large sample

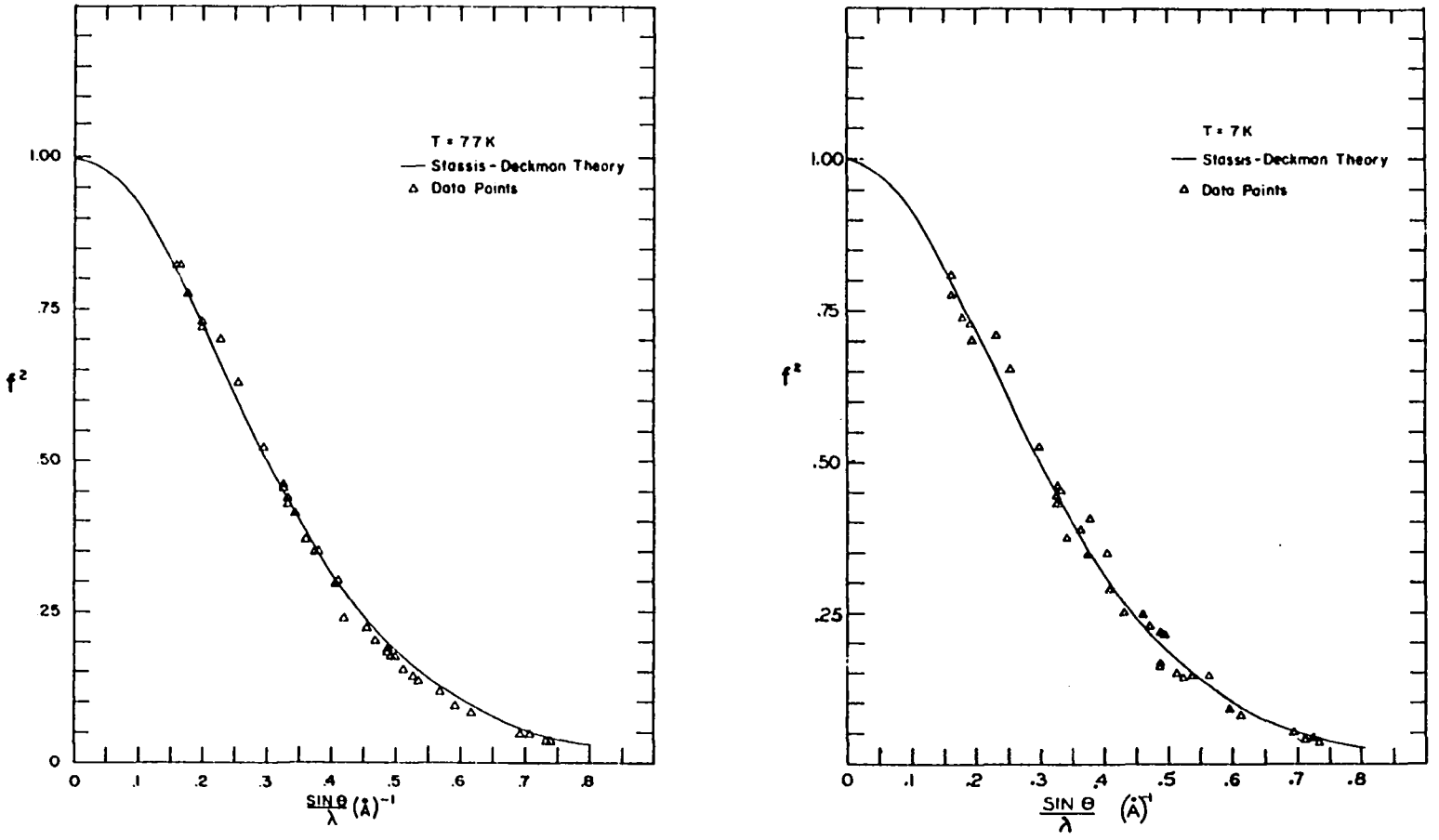

Figure 3.9. First order form factors

were related to the first order satellites from the small sample via the (300) fifth and seventh order satellites in both samples.

The third order form factor measurements were performed at T = 24K since at this temperature the $(300)^{+5}$ was well-separated from the $(302)^{-7}$ (and the $(300)^{+7}$ from the $(302)^{-5}$). The measured values are compared with the calculated form factor $[\frac{(B_2 + B_4)^2}{4}]$ for $\phi = \frac{\pi}{2}$ (see Figure 3.10). For $\phi = 0$ the third order form factor is zero and the measured points were along (hoo) or close to it.

Note the anomalously high $(100)^{+3}$ reflection. This reflection was stronger than predicted at all temperatures measured and followed roughly the temperature dependence of the $(300)^{\pm 3}$. A Renninger type of experiment, where the sample is rotated about the scattering vector, was performed to determine if the added intensity was due to multiple scattering effects. It was not.

The temperature dependence of the $(300)^{\pm 3}$ is shown in Figure 3.11. Between 30K and 60K no data are presented because the $(300)^{\pm 3}$ were lost in the background and could not be separated from it. The temperature dependence of the third order satellites measured here agrees qualitatively with the previous measurements[7].

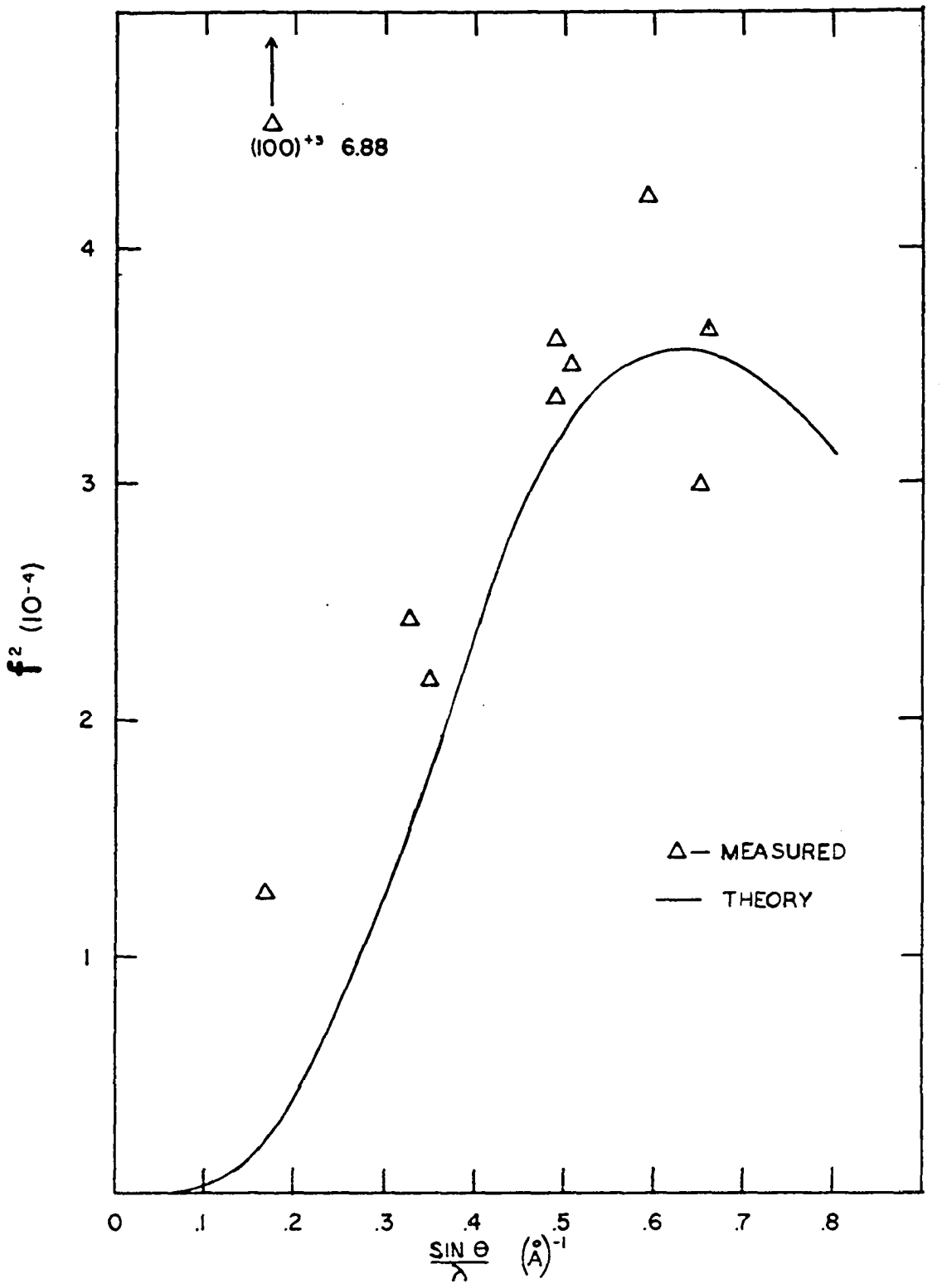

Figure 3.10. Third order form factors

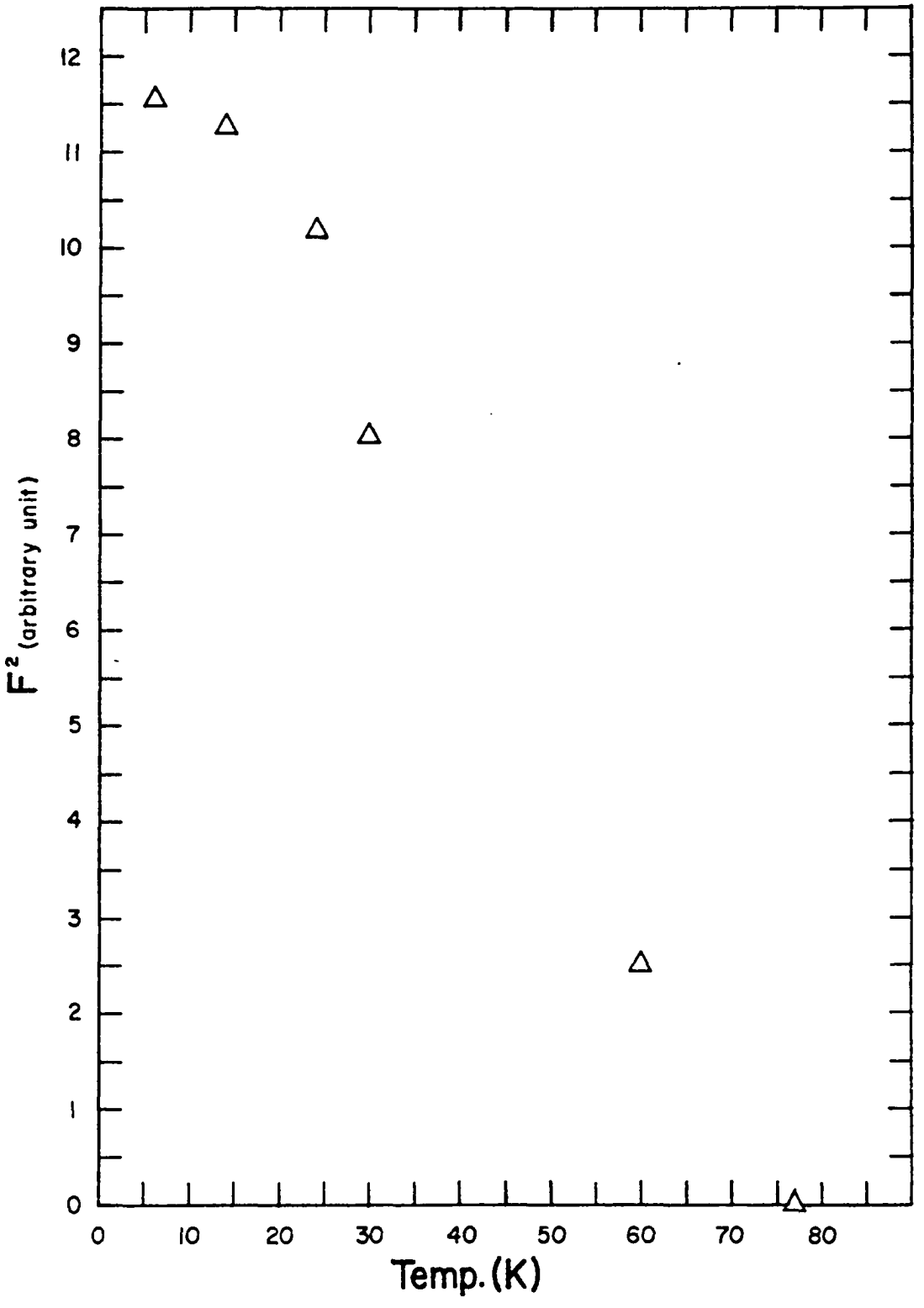

Figure 3.11. Third order structure factor vs. temperature

CHAPTER IV. DISCUSSION

This present work has been a detailed study of the magnetic structure versus temperature of a high purity, single crystal of metallic holmium. The results indicate that the Koehler et al.[6] sample B represented most accurately the magnetic properties of pure holmium metal. Both Koehler's sample B and the sample used in this present work were prepared by Ames Laboratory and are of very high purity. A careful study has quite well-established that the third order satellites are due to the asphericity of the ionic magnetization density. This asphericity arises because of the contribution of higher order multipole terms to the atomic form factor. Some questions still remain, however, due to the anomalously large $(100)^{+3}$ satellite.

The first order form factor calculated using the Stassis et al. multipoles agreed very well with measurements made both in this experiment and by Koehler et al. on Ho_2O_3.[6] It would be interesting to see if the calculated asymmetry of the form factor would be supported by careful measurement of several reflections along the [h00] and [00ℓ] directions respectively. It should also be noted that the form factor calculated here $(B_o + \frac{B_2}{2})^2$, differs from Felcher's calculations, $(B_o^2 + \frac{B_2^2}{4})$. The cross terms arise from considering explicitly the complex conjugate of basal plane moment.

The fifth and seventh order measurements showed good agreement with the measurements of Felcher et al.[7] except below the Curie temperature where in the present sample the magnetic unit cell became commensurate with 6 times the chemical unit cell (this was also the case with Koehler's B sample). Because fifth and seventh order satellites become superimposed

when this happens any information about the moment magnitude modulation is lost. Therefore it is not possible to tell if raising the moment out of the basal plane changed the crystal field effects upon the structure.

The magnetic periodicity showed changes of curvature at roughly 4, 5 and 6 times the chemical cell periodicity. This curve was highly reproducible upon repeated warming and cooling of the sample. The magnetic spiral structure is a result of crystal field effects on the moments in each layer being coupled to the crystal field effects on moments in adjacent layers via the indirect exchange interaction. This indirect exchange is mediated by the conduction electrons. These electrons form Fermi surfaces which reflect the symmetry existing in the lattice. The magnetic periodicity, while non-commensurate with the chemical unit cell, decreases the lattice symmetry and the Fermi surface is distorted. When the magnetic periodicity becomes commensurate with an integer multiple of the chemical unit cell the lattice symmetry is increased and the Fermi surface becomes less distorted. The theory by Elliott and Wedgewood[8] assuming a free electron (spherical) Fermi surface predicts the general slope of the magnetic periodicity temperature dependence. An examination of the change in sign of the curvature $\left[\frac{d^2 q_z}{dT^2}\right]$ as the magnetic periodicity becomes commensurate with an integer multiple of the chemical periodicity could well lead to a greater understanding of the indirect exchange interaction between adjacent basal plane layers of atoms

Of final interest are the observed differences in first order moment intensities between the [h00] and [00ℓ] directions (see Figure 3.7). This would seem to indicate an additional moment modulation along the c axis

that would not be picked up by the (00ℓ) reflections. It follows from this that below $\simeq$ 100K there is a small $\underline{c}$ axis modulation with the same periodicity as the basal plane modulation.

The observance of an anomalously high $(100)^{+3}$ satellite (see Figure 3.10) could be evidence that this $\underline{c}$ axis modulation deviates from purely sinusoidal as was found in erbium by Habenschuss et al.[9]

APPENDIX A

Reciprocal Space

In real space the lattice points in a crystal are given by

$$\rho_{mnp} = m\vec{a} + n\vec{b} + p\vec{c}$$

where m, n and p are integers and $\vec{a}$, b and $\vec{c}$ are basis vectors of the crystal lattice (see Figure 1.1 for hcp lattice). Radiation incident upon the crystal with wave vector $\vec{k}$ ($k = 2\pi/\text{wavelength}$) is scattered in a different direction with wave vector $\vec{k}'$. Scattering from each point produces a phase change in the radiation given by $e^{i\Delta\vec{k}\cdot\vec{\rho}}$, where $\Delta\vec{k} = \vec{k}'-\vec{k}$ and is called the scattering vector. When phases from all points add constructively (coherent scattering) a diffraction peak results. This occurs when

$$\sum_{\text{all points}} e^{i\Delta\vec{k}\cdot\vec{\rho}} = \text{maximum},$$

and this happens when

$$\Delta\vec{k}\cdot\vec{a} = 2\pi h,$$
$$\Delta\vec{k}\cdot\vec{b} = 2\pi k,$$
$$\Delta\vec{k}\cdot\vec{c} = 2\pi \ell,$$

where h, k and ℓ are indices called miller indices. Therefore, one can define points in reciprocal space by vectors

$$\vec{G} = h\vec{A} + k\vec{B} + \ell\vec{C},$$

where

$$\vec{A} = 2\pi \frac{\vec{b}\times\vec{c}}{\vec{a}\cdot\vec{b}\times\vec{c}} \; ; \; \vec{B} = 2\pi \frac{\vec{c}\times\vec{a}}{\vec{a}\cdot\vec{b}\times\vec{c}} \; ; \; \vec{C} = 2\pi \frac{\vec{a}\times\vec{b}}{\vec{a}\cdot\vec{b}\times\vec{c}}$$

and $\vec{A}$, $\vec{B}$ and $\vec{C}$ are the fundamental vectors of the reciprocal space. Note that $\vec{G}$ is a property of the crystal, with h, k and ℓ defining planes of atoms normal to the scattering vector, whereas the observation of $\Delta\vec{k}$ is determined, in practice, by the spectrometer angles. The diffraction condition, $\Delta\vec{k} = \vec{G}$, in effect states that when the spectrometer position coincides properly with the sample position coherent scattering results. For elastic scattering $\Delta\vec{k} = \vec{G}$ reduces to $n\lambda = 2d \sin\theta$ (Bragg's law).

APPENDIX B

Discussion of Magnetic Ordering Theory

The magnetic structure of holmium is produced by the combined influences of the crystal field (and its anisotropy), the indirect exchange interaction and magnetoelastic interaction. The total Hamiltonian is written

$$H = H_{ex} + H_{c.f.} + H_{me}.$$

The indirect exchange is the interaction of one localized 4f moment with a neighboring 4f moment via the conduction electrons. The Hamiltonian can be expressed in the Heisenberg form as[10]

$$H_{ex} = -(g_J-1)^2 \sum_{i\neq j} j(\vec{R}_i-\vec{R}_j)\vec{J}_i\cdot\vec{J}_j$$

where $j(\vec{R}_i-\vec{R}_j)$ is the exchange interaction between moments $\vec{J}_i$ and $\vec{J}_j$ located at lattice sites $\vec{R}_i$ and $\vec{R}_j$, and g_J is the Lande factor of moment J. Under certain approximations the exchange interaction can be expressed as

$$j(\vec{R}_i-\vec{R}_j) = \frac{2}{N^2} \sum_{\vec{q}} |U(\vec{q})|^2 \chi(\vec{q})\ e^{i\vec{q}\cdot(\vec{R}_i-\vec{R}_j)},$$

where $|U(\vec{q})|^2 \chi(\vec{q})$ is a weighted response function[11] for the conduction electrons and depends upon the shape of the Fermi surface of the metal in consideration.[12] The wave vector, $\vec{q}$, which maximizes the response function is the wave vector of the periodicity which stabilizes the magnetic structure. The exchange Hamiltonian written here is isotropic with respect to spin in real space but in actuality there are small effects[10] arising

from anisotropy in 4f and conduction electron wave functions which give rise to anisotropy in the indirect exchange interaction.

The 4f electrons on each ion are situated in an inhomogeneous electrostatic potential arising from the other ions and conduction electrons in the solid. This potential gives rise to a field known as the crystal field. The symmetry (anisotropy) of the crystal field is determined by the crystallographic structure of the solid.

The potential experienced by a single ion is due to its neighbors can be expanded in terms of spherical harmonics about the center of the test ion as follows

$$V(r,\theta,\phi) = \sum_{\ell,m} \gamma_{\ell m} r^{\ell} Y_{\ell}^{m}(\theta,\phi)$$

where $\gamma_{\ell m}$ depend upon the distribution of neighboring charges around the test ion. This can be rewritten (via an angular momentum transformation) in a more convenient form,[13]

$$H_{c.f.} = \sum_{i\ell m} B_{\ell m} O_{\ell}^{m}(\vec{J}_i)$$

where:

$$B_{\ell m} = \alpha_{\ell} \gamma_{\ell m} \langle r^{\ell} \rangle$$

α_{ℓ} is the Stevens factor and reflects the anisotropy of the test ion's charge distribution,

$\langle r^{\ell} \rangle$ are the expectation values of the radial 4f electrons,

$O_{\ell}^{m}(\vec{J}_i)$ are operators equivalent to the corresponding spherical harmonics (same ℓ and m) but with argument J_x, J_y and J_z instead of x, y and z.

The number of terms actually allowed in this sum is determined by the point group symmetry of the site and the f(ℓ=3) electron orbitals. For hexagonal crystal structure these terms are[14]

$$H_{c.f.} = B_{20} O_2^0 + B_{40} O_4^0 + B_{60} O_6^0 + B_{66} O_6^6 \ .$$

The first three terms relate to the crystal field anisotropy along the crystallographic c axis and the last term relates to the basal plane anisotropy. The signs and magnitudes of the $B_{\ell m}$ coefficients give the relative magnitudes and directions to various crystal field anisotropy terms.

The $B_{66} O_6^6$ term gives rise to the bunching of the moments in the basal plane below 50 K in holmium. That the bunching dies away so quickly with increasing temperature can best be understood in light of the strong temperature dependence of B_{66}. The anisotropy coefficient at temperature, T, is related to the same at T=0 by[15]

$$\frac{K_\ell(T)}{K_\ell(0)} = \left[\frac{m(T)}{m(0)}\right] \frac{\ell(\ell+1)}{2}$$

where m(T) is the sublattice magnetic moment. Because the basal plane anisotropy has ℓ=6 whereas the leading axial anisotropy term has ℓ=2 the basal plane anisotropy will decrease with increasing temperature as $\left[\frac{m(T)}{m(0)}\right]^{21}$ while the axial anisotropy decreases as $\left[\frac{m(T)}{m(0)}\right]^{3}$. This means that above a certain temperature, approximately 50 K for holmium, the six fold anisotropy has negligible influence on the magnetic ordering. As a result, the bunching effect vanishes while the moments are still constrained in the basal plane by the axial anisotropy.

Magnetostriction in a solid is a dimensional distortion caused by the coupling of magnetic moments to the crystal lattice. The Hamiltonian can be written very generally as[16]

$$H_{me} = \left[\frac{\partial E_{c.f.}}{\partial \epsilon_{ij}} + \frac{\partial E_{ex}}{\partial \epsilon_{ij}} + \cdots\right] \epsilon_{ij}$$

where ϵ_{ij} represents the strain present in the system. This is a phenomenological expression and in general the strain derivatives of the crystal field energy and exchange energy will be treated as adjustable parameters. The number of terms appearing in the Hamiltonian will depend upon the symmetry of the crystal structure. The symmetry selection here is similar to the symmetry selection of terms in the crystal field Hamiltonian, and as a result the $\frac{\ell(\ell+1)}{2}$ power law[15] governs the temperature dependence of the magnetoelastic contribution to the total energy. The magnetoelastic energy and the planar crystal field anisotropy tend to stabilize a ferromagnetic structure whereas the exchange interaction prefers the spiral antiferromagnetic structure.[16] Because of the $\frac{\ell(\ell+1)}{2}$ power law, the planar crystal field anisotropy and the magnetoelastic energy rise sharply with decreasing temperature at low temperatures, whereas the exchange interaction varies less rapidly with temperature. These two tendencies compete as the temperature is decreased until, at 20 K in holmium, a ferromagnetic component is produced along the c axis. This transition was reflected in the lattice parameter measurements (see Figure 3.5).

Evenson and Liu,[17] using a simple but general model for magnetostriction in a helical structure, showed that the temperature variation of the lattice parameters was due to a "clamping" effect by the first few

layers of atoms closest to the surface of the sample volume. This clamping also gives more insight into the antiferromagnetic to ferromagnetic transformation. In the helical structure only a few atomic layers on the surface can respond to the magnetostriction and as a result there is no reduction of bulk free energy. With the introduction of a ferromagnetic component at each atomic site, the whole lattice can respond to magnetostriction and because of a reduction in total free energy the ferromagnetic structure becomes stable.

BIBLIOGRAPHY

1. C. Stassis, H. W. Deckman and B. N. Harmon, Phys. Rev. B15, 369 (1977).

2. C. Stassis and H. W. Deckman, J. Phys. C9, 2241 (1976).

3. M. Rotenberg, R. Bivins, N. Metropolis, J. Wooten, Jr., The 3-j and 6-j Symbols (Technology Press, Cambridge, 1959).

4. Y. A. Izyumov and R. P. Ozerov, Magnetic Neutron Diffraction (Plenum Press, New York, 1970).

5. International Tables for X-ray Crystallography (Kynoch Press, Birmingham, England).

6. W. C. Koehler, J. W. Cable, M. K. Wilkinson and E. O. Wollan, Phys. Rev. 151, 414 (1966).

7. G. P. Felcher, G. H. Lander, and T. Arai, Phys. Rev. B13, 3034 (1976).

8. R. J. Elliott and F. A. Wedgewood, Proc. Phys. Soc., London 84, 63 (1964).

9. M. Habenschuss, C. Stassis, S. K. Sinha, H. W. Deckman and F. H. Spedding, Phys. Rev. B10, 1020 (1974).

10. S. K. Sinha, Chapter 7, Handbook on the Physics and Chemistry of Rare Earths, K. A. Gschneidner, Jr. and L. Eyring, eds. (North Holland Publishing Co., Amsterdam, 1978).

11. B. N. Harmon and A. J. Freeman, Phys. Rev. B10, 4849 (1974).

12. S. H. Liu, Chapter 3, Handbook on the Physics and Chemistry of Rare Earths, K. A. Gschneidner, Jr. and L. Eyring, eds. (North Holland Publishing Co., Amsterdam, 1978).

13. K. W. H. Stevens, Proc. Phys. Soc. A65, 209 (1952).

14. K. N. R. Taylor and M. I. Darby, Physics of Rare Earth Solids (Chapman and Hall Ltd., London, 1972).

15. H. B. Callen and E. Callen, J. Phys. Chem. Solids 27, 1271 (1966).

16. B. R. Cooper, Chapter 2, Magnetic Properties of Rare Earth Metals, R. J. Elliott, ed. (Plenum Press, London and New York, 1972).

17. W. E. Evenson and S. H. Liu, Phys. Rev. 178, 783 (1969).

ACKNOWLEDGMENTS

The author would like to thank, Professor C. Stassis for his guidance and encouragement and for the opportunity to work in his neutron scattering group, and also Professors S. Liu and B. Harmon for their enlightening discussions about the theory of magnetic ordering in the rare earths. The author would also like to thank God for revealing His nature to us all.

"And He is before all things, and in Him all things hold together,"

Colossians 1:17